Palaeogeography, Palaeoclimatology, Palaeoecology 660 (2025) 112700

Contents lists available at ScienceDirect

Palaeogeography, Palaeoclimatology, Palaeoecology

journal homepage: www.elsevier.com/locate/palaeo

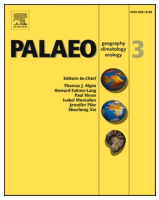

Source-rock, grain-size, weathering, and recycling controls on the feldspar/quartz ratio in silt-sized sediments

Hanjing Fu, Xing Jian *, Zhihua Zhang, Hanqing Pan

State Key Laboratory of Marine Environmental Science, College of Ocean and Earth Sciences, Xiamen University, Xiamen 361102, PR China

ARTICLE INFO

Editor: Howard Falcon-Lang

Keywords:
River sediments
Silt-sized minerals
Chemical weathering
Lithology
Sediment recycling

ABSTRACT

Numerous chemical weathering indices have been proposed based on analyses of weathering products and/or residues from siliciclastic sediments to reconstruct paleoclimate. The subjects of weathering studies often concentrate on the bulk-sample, clay and sand components, neglecting the study of silt mineral composition and its potential applications in weathering and provenance analysis. In this study, we investigate the variability of the plagioclase/quartz (Pl/Qtz), feldspar/quartz (F/Qtz), K-feldspar/quartz (Kfs/Qtz), plagioclase/K-feldspar (Pl/Kfs) ratios in silt-sized fractions of siliciclastic sediments of East Asian rivers to understand superimposed controlling factors of lithology, climate, recycling and grain size. Results indicate that the Pl/Qtz and F/Qtz ratios of silt-sized sediments from representative rivers in East Asia show significant correlations with climatic factors (R^2: 0.48–0.82), with a Pl/Qtz ratio of 0.3 differentiating dry-cold climates (Pl/Qtz > 0.3) and wet-warm climates (Pl/Qtz < 0.3). Given the substantial influence of felsic-mafic parent rock lithology and polycyclic quartz enrichment on silt-sized mineral ratios, along with the intricate geological context of the global river data collected, it follows that the silt-sized mineral composition in global river sediments exhibits a limited climate-weathering control and a weak correlation with temperate and precipitation. Grain size bias is evident in silt component, with compositional differences between the 2–32 μm and 32–63 μm fractions mainly attributed to the varying chemical-physical abrasion properties of quartz, K-feldspar, and plagioclase, and potentially linked to size inheritance from parent rocks. To enhance the accuracy of weathering and provenance analysis, we recommend conducting sediment grain size differentiation and multi-grain size studies, focusing on the extent of weathering and provenance signals in mineral composition, and emphasizing the integrated application of various chemical weathering indices.

1. Introduction

Silicate chemical weathering is a fundamental geological process on the Earth's surface and closely intertwined with carbon cycling, which has long been regarded as the Earth's thermostat. Chemical weathering involves the utilization of CO_2 and H_2O to decompose primary minerals in fresh rocks, and concurrently releasing dissolved substances into fluids and forming secondary minerals (Frings and Buss, 2019; Brantley et al., 2023; Hilton, 2023). Siliciclastic sediments/sedimentary rocks are composed of both weathering residues and newly formed weathering products. Weathering residues consist of partially weathered or unaltered primary minerals such as quartz, feldspars and micas, whereas, weathering products include secondary clay minerals that form as a result of weathering, like kaolinite, illite, smectite and chlorite (Wilson, 2004;Van De Kamp, 2010). Because of the different weathering stability of minerals and weathering behavior of elements (Worthington et al., 2016; Ma et al., 2007), the chemical weathering intensity indices are mainly calculated based on the proportion of the mineralogical, elemental and isotopic compositions in weathering residues and products within sediments, providing a quantitative evaluation of sediment chemical weathering intensity. For examples, petrological (e.g., quartz (Q)-feldspar (F)-lithics (L) plot of sandstones), clay mineralogical (e.g., kaolinite/illite, illite crystallinity index), elemental (e.g., Chemical Index of Alteration, Chemical Index of Weathering, Plagioclase Index of Alteration, αE, α^{Al}Na, Rb/Sr), isotopic (e.g., δ^7Li, δ^{41}K) and textural (e.g., surface textures of heavy minerals) indicators (Nesbitt and Young, 1982; Harnois, 1988; Fedo et al., 1995; Gaillardet et al., 1999; Jin et al., 2006; Kamp, 2010; Alizai et al., 2012; Andò et al., 2012; Garzanti et al., 2013b; Dinis et al., 2020; Teng et al., 2020; Gou et al., 2024).

Mineral and chemical compositions of siliciclastic sediments/

* Corresponding author.
E-mail address: xjian@xmu.edu.cn (X. Jian).

https://doi.org/10.1016/j.palaeo.2024.112700
Received 18 October 2024; Received in revised form 30 December 2024; Accepted 30 December 2024
Available online 2 January 2025

sedimentary rocks are shaped not only by weathering but also by multiple geological factors in sediment source-to-sink system, e.g., sediment grain size (Jian et al., 2013), parent rock lithology (von Eynatten et al., 2016), diagenesis and recycling (Guo et al., 2018). The most widely used major-element weathering indices are primarily controlled by mineral compositions (Fu et al., 2023) and involve both weathering residues and weathering products, resulting in several biases in chemical weathering intensity evaluation. Detrital clay mineral assemblages and crystallographic indices focus on weathering products and reflect first-cycled or inherited climate-driven weathering intensity due to different formation conditions of kaolinite, illite, smectite and chlorite (Goodfellow, 2012; Song et al., 2023; Wang et al., 2023). Weathering indices based on weathering residues include petrological compositions in sandy sediments (63 μm–2 mm, Kamp, 2010; Blott and Pye, 2012) and the Mineralogical Index of Alteration (MIA, Rieu et al., 2007; Hessler et al., 2017) dependent on the proportions of quartz and feldspar. It is noteworthy that quartz, plagioclase and K-feldspar have similar density ranges (2.56–2.71 g/cm^3) (Garzanti et al., 2008, 2009) and different weathering priority (plagioclase > K-feldspar > quartz, Kamp, 2010) make mineral ratios (feldspar/quartz, plagioclase/quartz, K-feldspar/quartz, plagioclase/K-feldspar) theoretically effective proxies for evaluation of chemical weathering intensity. However, multiple controls (e.g., lithology, grain size, recycling) on quartz and feldspar content in sediments imply that MIA may be not a robust indicator in climate-driven weathering (Dinis et al., 2020). For example, both the fluvial sands from the hyper-humid Congo basin and the dune sands from the hyper-arid Sahara and Arabian deserts show high "MIA" values (ca. 100) (Muhs, 2004; Garzanti et al., 2013c).

The influence of non-weathering factors on the composition of coarse-grained sediments is greater than that on fine-grained sediments (Guo et al., 2021). Thus, does the enhanced preservation of weathering signals in fine-grained sediments improve the reliability of using mineralogical indicators, such as the feldspar/quartz ratio, to assess the intensity of chemical weathering? To address this question, we choose the silt component of fine-grained sediments to be the study subject, rather than the clay component. Clay or mud are mainly composed of weathering products (i.e., clay minerals), phyllosilicates and quartz (Nyakairu and Koeberl, 2001; Adriaens et al., 2018), and the associated researches on clay minerals have been well-established (Li et al., 2012; Setti et al., 2014). In comparison, silty sediments contain weathering residues and also have less lithic fragments interference compared to sandy sediments, which aids in the more accurate determination of the contents of quartz, K-feldspar, and plagioclase (Tolosana-Delgado and von Eynatten, 2009; Caracciolo et al., 2012; Borromeo et al., 2019). Additionally, grain size distributions of siliciclastic geological archives, including global soils, marine and fluvial sediments, indicate that silt component occupies the largest proportion in most samples compared to sand- and clay-sized detritus (Fig. 1, Table S1, Assallay et al., 1998). The high flux of silt makes it a crucial component in sediment source-to-sink analysis and in the reconstruction of paleo-weathering, paleoclimate and paleoenvironment.

Current researches primarily focus on the geochemical composition of silt-sized sediments (2–63 μm) but overlooks the mineralogical study of the silty fraction (Dekov et al., 1997; Bouchez et al., 2011; Garzanti et al., 2014b), with only a few case studies (Garzanti et al., 2011). Previous studies by Yang et al. (2008) have investigated the silt-sized

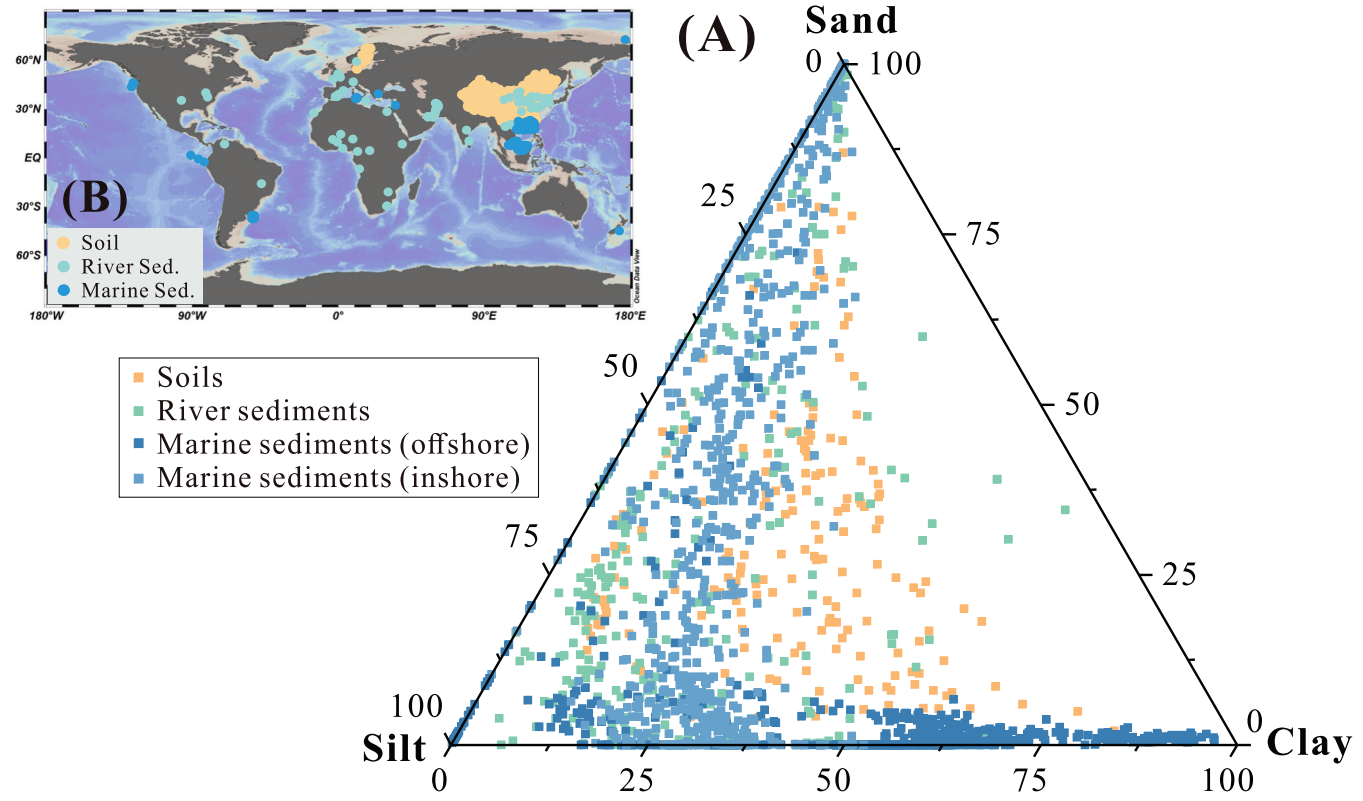

Fig. 1. Grain size distribution of global soils ($n = 426$), river sediments ($n = 273$), marine sediments ($n = 1397$) (A) and sample sites (B). Soil samples were collected mainly from Sweden and China (Keller and Håkansson, 2010; Shangguan et al., 2013; Xu et al., 2013; Peng et al., 2014). The global river sediments sampled from both riverbed and floodplain (Lim et al., 2006; Manassero et al., 2008; Luo et al., 2012; Venkatramanan et al., 2013; Mutema et al., 2015; Pan et al., 2015; Zhou et al., 2015; Hou et al., 2021). Marine surface and core sediments mainly came from the South China Sea, Mediterranean Sea, Pacific Ocean, Atlantic Ocean and Arctic Ocean (Wan et al., 2007; Hamann et al., 2008; Land et al., 2010; Gutiérrez-Pastor et al., 2013; Szczuciński et al., 2013; Franco-Fraguas et al., 2014; Wang et al., 2014; Brahim et al., 2015; Bista et al., 2016; Xu et al., 2017; Zhong et al., 2017; Swärd et al., 2018; Huang et al., 2021; Hu et al., 2024; Yu et al., 2024). Marine sediments are mainly located on the continental shelf and slope, and further divided into inshore and offshore sediments. In most soil, river and marine sediment samples, the content of silt components is higher than that of sand and clay. Specific information and data refer to Table S1.

mineral ratios of sediments from the Yangtze and Yellow rivers, showing strong correlations between feldspar/quartz (F/Qtz), plagioclase/quartz (Pl/Qtz), K-feldspar/quartz (Kfs/Qtz) ratios and climate-driven chemical weathering intensity. However, the diverse array of climatic conditions and complex lithological compositions within the Yangtze and Yellow rivers basins (Wang et al., 2019) presents challenges in discerning the influence of confounding factors. There is a lack of comprehensive analysis and understanding of the significance of these tectosilicate mineral ratios in fine-grained sediments. The quantitative relationships between climate and silt-sized mineral indices at both global and regional scales are not yet fully understood and warrant further investigation.

This study introduces new mineralogical data from silt-sized sediments of modern rivers across East Asia, which span from tropical to cold climatic zones, and also consolidates previously published silty mineralogical data from global river sediments. The rivers in East Asia

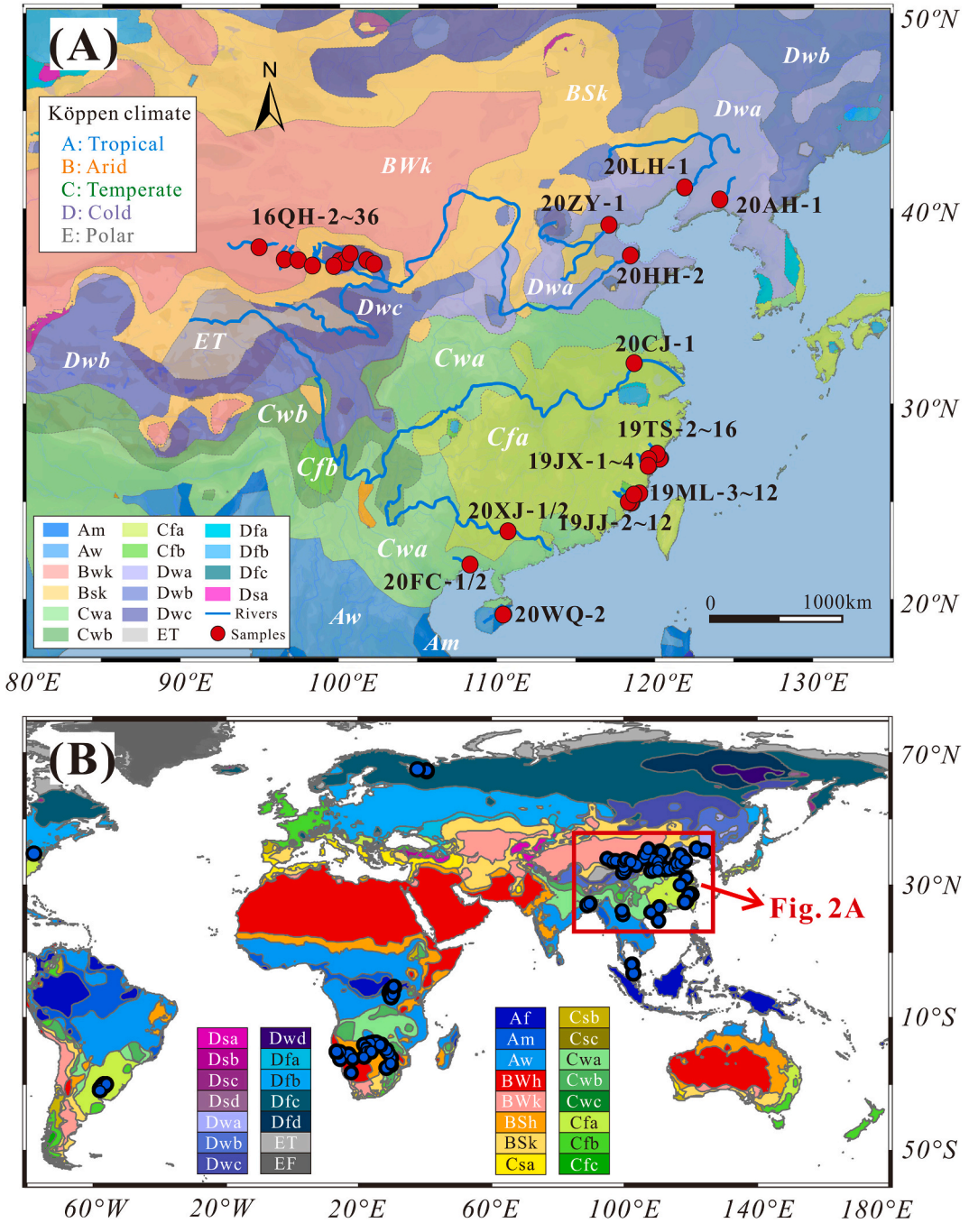

Fig. 2. Global distribution of Köppen-Geiger climate types and the locations of the river sediments in East Asia analyzed in this study (A) and the associated global river sediments/SPM (B). Mineralogical data for the global samples were obtained from published studies (Bhuiyan et al., 2011; Ding et al., 2011; Garzanti et al., 2011, 2014, 2015, 2021; Zhou et al., 2015; Singleton et al., 2017; Wu et al., 2019, 2022; Nemirovskaya and Shevchenko, 2020; Tian et al., 2021; Gordeev et al., 2022), and references for climate information are given in the Table S2. Letter designations for climates is from Köppen-Geiger climate classification (Peel et al., 2007). Af = tropical rainforest; Am = tropical monsoon; Aw = tropical savannah; BWh/BWk = arid hot/cold desert; BSh/BSk = arid hot/cold steppe; Cwa = temperate with dry winter and hot summer; C = temperate, D = cold, E = polar; s = dry summer, w = dry winter, f = without dry season; a = hot summer, b = warm summer, c = cold summer, d = very cold winter; T = tundra, F = frost. The description and criteria for all climate types are shown in Table S3.

we focused are mainly small catchments with relatively simple lithology across various climate conditions. The aims are (1) to quantify the relationship between the silt-sized mineral ratios (i.e., F/Qtz, Pl/Qtz, Kfs/Qtz and Pl/Kfs) and climate-driven chemical weathering; (2) to compare the preservation of weathering signals in fine-grained sediments between East Asian rivers and a global context; (3) to analyze the multiple geological factors such as source rock lithology, grain size and recycling effect on the silt-sized mineral composition in river sediments, and to discuss the controlling mechanisms.

2. Material and methods

2.1. Samples and data collection

A total of 48 fluvial sediment samples were collected for mineralogical analysis in this study from 20 rivers in East Asia, covering tropical (Am), arid (BSk, BWk), temperate (Cfa, Cwa) and cold (Dwa, Dwc) climatic conditions (Fig. 2A), with mean annual temperature (MAT, 2000–2021 AD) ranging from 0 to 25 °C and mean annual precipitation (MAP) ranging from 77 to 2102 mm (climate data from National Earth System Science Data Center, National Science & Technology Infrastructure of China, http://www.geodata.cn). Although, the silt-sized mineral ratios have been confined to 2–63 μm components, there may still be potential grain size interference. In order to investigate the grain size effect on the silt-sized mineral ratios, we separate the samples into two subfractions of 2–32 μm and 32–63 μm, and yield 96 sets of data (Table S2). In addition to new sample analysis data, we also compiled mineralogical data of silt-sized sediments/suspended particulate matter (SPM) from global rivers (205 sets of data) from literatures. These samples are mainly located in Asia and Africa and cover various climatic conditions (Fig. 2B). For specific information on all samples, refer to Supplemental Material Table S2. The climate regions are categorized according to the Köppen-Geiger climate classification system (Table S3, Peel et al., 2007). This system employs three-letter symbols that consider temperature and precipitation as key indicators and are linked to the types of natural vegetation found in the area. The first letter denotes the primary climate groups: tropical (A), arid (B), temperate (C), cold (D), and polar (E). The second letter describes the distribution of annual or seasonal precipitation, and the third letter indicates the pattern of annual or seasonal temperatures (Zeroual et al., 2019; Wu et al., 2021). A detailed description of the Köppen–Geiger climate classification is provided in Table S3.

2.2. Analytical methods

2.2.1. Extraction and compositional analysis of silt fraction

Approximately 100 g of each sediment sample was wet sieved through 240 mesh and 480 mesh nylon mesh to obtain 32–63 μm and < 32 μm detrital components and then dried. About 7–8 g of dried <32 μm samples, deionized water and 0.1 g $(NaPO_3)_6$ were added into a 100 ml centrifuge tube and dispersed for 30 min by using an ultrasonic oscillator to prevent flocculation and precipitation of clay minerals. Based on Stokes' law, the settling time for particles of 2 μm to reach a certain depth was determined, and once this time elapsed, the corresponding particle fractions were extracted and concentrated in a centrifuge. Equation of settling velocity (1) based on the Stokes' law are as follows (Stokes, 1850; Maggi, 2013), where v is particle settling velocity, cm/s, ρ is particle density, g/cm^2, σ is water density, g/cm^2, r is particle radius, cm, η is fluid viscosity coefficient, Pa·S, g is gravity acceleration, cm/s^2.

$$v = 2gr^2 (\rho - \sigma)/9\eta \quad (1)$$

To remove organic matter and carbonate in the samples, 30 ml 10 % H_2O_2 and 1 mol/L CH_3COOH were successively added to the separated fractions and heated in a water bath at 60 °C for 1 h and 4 h, respectively. The remaining materials were centrifuged to remove the excess reaction liquid and dried. After completion of the above steps, the 2–32 μm and 32–63 μm sample powders were analyzed by X-ray diffraction (XRD) (Ultima IV) at Xiamen University. Each sample was scanned continuously under conditions of 40 kV, 30 mA, wavelength of 1.54 and step width of 0.02°. Scanning angles and speeds were 5–60° and 4°/min, respectively (Fu et al., 2022).

JADE 6.0 software was used for identification and quantification of minerals in samples by the RIR method (Reference Intensity Ratio). The RIR method is carried out by the intensity of the strongest single diffraction peak of each mineral phase with the RIR value (Xiao et al., 2023). The RIR value ($I_i/I_{(113)cor}$) is determined based on the intensities of the most intense corundum (pure a-Al_2O_3, as an internal standard) reflection ($I_{(113)cor}$) and the target mineral reflection (I_i) in a 50:50 mixture by weight (Hillier, 2000; Zhou et al., 2018). The most intense peaks of measured minerals are as follows, quartz (3.34 Å), K-feldspar (3.24 Å), Na—Ca plagioclase (3.18–3.20 Å), kaolinite (7.19 Å), illite (10 Å) and chlorite (14.2 Å) (Mei et al., 2021). The RIR value of each mineral refers to JADE-PDF-2004.

2.2.2. Petrographic analysis

The 250–500 μm fractions of the river sediment samples (sand component) were impregnated with araldite and then standard thin sections of 30 μm thickness were prepared for observation under a polarizing microscope. The percentages of framework grains (i.e., quartz, feldspar and lithic fragments) were counted by the Gazzi-Dickinson method (Ingersoll et al., 1984; Zuffa, 1985; Jian et al., 2023).

2.2.3. Clay mineral analysis

Clay fractions (<2 μm) of the river sediment samples were separated according to Stoke's law, and organic materials and carbonate therein were removed by 10 % H_2O_2 and 1 mol/L CH_3COOH, respectively. The wet concentrated particles were placed on glass slides to produce air-dried oriented mounts. The oriented mounts were then saturated with ethylene glycol vapor for 48 h. Each sample was continuously scanned by Ultima IV X-ray diffraction under 40 kV, 30 mA, wave length of 1.54 and step width of 0.02° conditions. Scanning angles and speeds were 4–35° and 10°/min, respectively (Mei et al., 2021). The relative proportions of smectite (Sme), illite (Ill), kaolinite (Kao) and chlorite (Chl) were determined from the ratios of the integrated peak areas of (001) series of their basal reflections according to the XRD diagrams of ethylene glycol treated mounts, and were weighted by empirically estimated factors (Mei et al., 2021). Illite chemistry index (CI) was calculated based on the ratio of the basal reflection peak area of illite 5 Å (002) and 10 Å (001) peaks (Esquevin, 1969).

3. Results

3.1. Petrographic results

Representative photomicrographs of sand components of the river sediments in East Asia refer to Fig. S1. We mainly focus on Qinghai (16QH-8) and Aihe (20AH-1) river sediments in the cold zone, Tongshanxi (19TS-12), Mulanxi (19ML-10), and Xijiang (20XJ-1) river sediments in temperate zone, and Wanquanhe (20WQ-2) river sediments in tropical zone (Fig. 2). The framework grains in sediments of Qinghai rivers are dominated by metasedimentary rock fragment (31 %), quartz (30 %) and carbonate (28 %). Sediment of the Aihe river is mainly composed of quartz (38 %), feldspar (29 %) and lithic fragments of igneous rocks (24 %), with minor pyroxene. Tongshanxi river is dominated by sedimentary rock fragment (56 %) and quartz (38 %). Mulanxi river, dominated by quartz (53 %), feldspar (18 %) and sedimentary rock fragment (23 %). Xijiang river sediment is dominated by quartz (68 %), with subordinate sedimentary rock fragment (21 %). Wanquanhe river sediment is mainly composed of quartz (41 %) and sedimentary rock fragment (22 %), followed by K-feldspar (11 %), plagioclase (11 %), and lithic fragments of igneous rocks (7 %) and metamorphic rocks

(8 %). The siliciclastic composition of river sediments in East Asia generally reflects that the parent rocks are dominated by felsic rocks, such as granite, granodiorite, siliciclastic rocks of felsic origin.

3.2. Silt-sized mineral composition

River sediments in East Asia are mainly composed of quartz, K-feldspar, plagioclase and clay minerals (i.e., kaolinite, illite and chlorite). Feldspar/quartz (F/Qtz), plagioclase/quartz (Pl/Qtz), K-feldspar/quartz (Kfs/Qtz) and plagioclase/K-feldspar (Pl/Kfs) ratios in 2–32 μm components are in ranges of 0.06–1.20 (average (AVG): 0.39), 0.03–0.77 (AVG: 0.23), 0.03–0.43 (AVG: 0.16) and 0.35–5.31 (AVG: 1.74), respectively (Fig. S2). Those ratios in 32–63 μm components are in ranges of 0.02–1.76 (AVG: 0.72), 0–1.20 (AVG: 0.38), 0.02–0.83 (AVG: 0.34), 0–3.05 (AVG: 1.20) (Fig. S2). The F/Qtz, Pl/Qtz and Kfs/Qtz ratios increase with the increase of sediment grain size. Conversely, the Pl/Kfs ratio is decrease with the increase of sediment grain size.

3.3. Clay mineral composition

Clay mineral assemblages of Qinghai rivers sediments (QH) generated in dry-cold climate and Fujian rivers sediments (Tongshan, Jiaoxi, Mulan, Jinjiang) produced in warm-wet climate were analyzed. The results show that smectite is almost absent in the above-mentioned river sediments (Fig. S3), with an average (AVG) of 0–2 % among the four main clay minerals (Fig. S3). There is no significant difference in chlorite content between Qinghai and Fujian rivers sediments (AVG:15–24 %). In the sediments of the Qinghai and Jiaoxi rivers, the abundance of illite is greater than that of kaolinite. Specifically, the sediments from the Qinghai rivers exhibit an average illite content of 68 %, in contrast to 10 % kaolinite. The Jiaoxi river sediments are characterized by an average illite content of 66 % and kaolinite content of 18 %. Conversely, the Jinjiang sediments are rich in kaolinite (AVG: 55 %) and relatively poor in illite (AVG: 25 %). The contents of kaolinite and illite in Tongshanxi and Mulanxi rivers are comparable. The average content of illite in sediments of both rivers is approximately 42 %, while the average content of kaolinite ranges from about 33 % to 38 %. (Fig. S3). The illite chemistry index in sediments from Qinghai rivers is generally below 0.4, whereas the index in sediments from the four Fujian rivers displays a broader range of variability, spanning from 0.3 to 0.6 (Fig. S8).

4. Discussion

4.1. Differential climate controls on silt-sized mineral composition

4.1.1. Strong climatic effects on silt-sized mineral ratios in East Asia rivers

Climate is considered to be one of the main external controls on the rate and intensity of silicate chemical weathering (Penman et al., 2020; Deng et al., 2022). The close relationship between sediment chemical weathering intensity and climatic factors (i.e., wetness and temperature) have underpinned numerous studies to reconstruct paleoclimate and paleoenvironment by focusing on the siliciclastic sediment compositions (Fu et al., 2022; Lv et al., 2022). Therefore, this study reflects the extent to which climate-driven weathering intensity affects the silt-sized mineral composition by analyzing the relationship between mineral ratios and mean annual temperature (MAT) and precipitation (MAP).

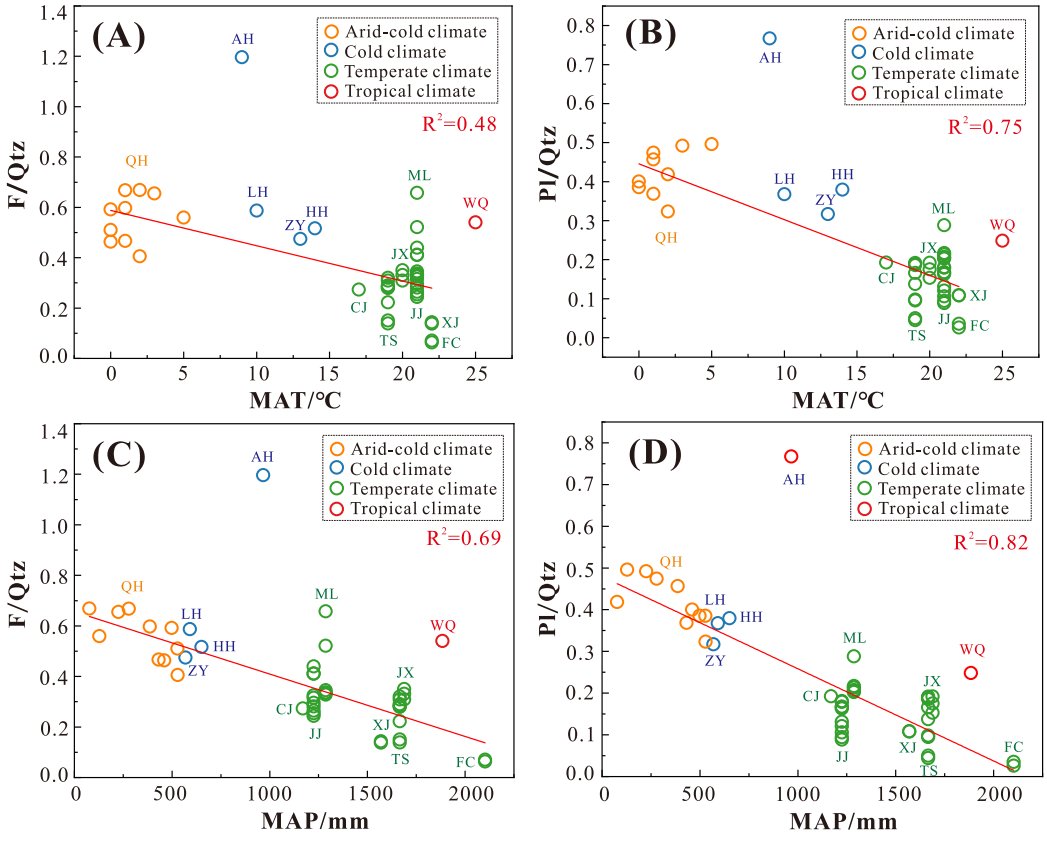

Fig. 3. Correlation between the mineral composition of 2–32 μm component and mean annual temperature/precipitation (MAT/MAP). F/Qtz: feldspar/quartz, Pl/Qtz: plagioclase/quartz. QH: Qinghai rivers, AH: Aihe river (tributary of the Yalu river), LH: Liaohe river, ZY: Ziya river (tributary of the Haihe river), HH: Yellow river, CJ: Yangtz river, TS: Tongshanxi river, JX: Jiaoxi river, ML: Mulanxi river, JJ: Jinjiang river, FC: Fangchengjiang river, XJ: Xijiang river (tributary of the Pearl river), WQ: Wanquanhe river. Among them, FC, XJ, WQ are at the lowest latitude, followed by CJ, TS, JX, ML and JJ, while QH, ZY, HH, AH and LH are at the highest latitude. For specific sample information, refer to Table S2. (For interpretation of the references to colour in this figure legend, the reader is referred to the web version of this article.)

The mineralogical results reveal that sediments originating from tropical and temperate climatic conditions typically exhibit diminished F/Qtz, Pl/Qtz, and Pl/Kfs ratios in comparison to those derived from arid-cold climatic regimes (Fig. 3, Fig. S4). Among these four mineral ratios, the Pl/Qtz and F/Qtz ratios are particularly sensitive to climatic factors. For instance, the correlation coefficient R^2 for Pl/Qtz with respect to temperature and precipitation ranges from 0.64 to 0.82, while that for F/Qtz spans from 0.4 to 0.8 (Fig. 3, Fig. S4). Due to the differences in weathering rates between K-feldspar and plagioclase, the Pl/Kfs ratio has a moderate correlation with climate (R^2: 0.38–0.47) (Fig. S4). Kfs/Qtz ratios in sediments of East Asian rivers are insensitive to climate and chemical weathering (Fig. S4). The reasons for the obvious difference between the four silt-sized mineral indices and climate factors are as follows. The collected sediments of East Asian rivers in this study were less exposed to extreme tropical weathering. Considering that plagioclase is more susceptible to weathering than K-feldspar (White et al., 2001), most samples have undergone the stage of plagioclase weathering to varying degrees, while K-feldspar in sediments has undergone relatively less weathering modification. As a result, the content of K-feldspar and the Kfs/Qtz ratio in sediments primarily reflect the material contribution from the parent rock, while climatic weathering exerts a relatively minor impact on Kfs/Qtz ratio and relatively strong impacts on F/Qtz and Pl/Qtz ratios.

Compared with the 32–63 μm fraction, mineral ratios in the 2–32 μm fraction demonstrate stronger correlations with climatic factors (Fig. 3; Fig. S4), Specifically, there are moderate correlations between F/Qtz and MAT ($R^2 = 0.48$) and MAP ($R^2 = 0.69$), and strong correlation between Pl/Qtz and MAT ($R^2 = 0.75$) and MAP ($R^2 = 0.82$) (Fig. 3). Therefore, the variability of the F/Qtz and Pl/Qtz ratios, particularly in the 2–32 μm fraction of sediments in East Asian rivers, largely reflects the intensity of climate-driven chemical weathering.

4.1.2. *Slight climatic effects on silt-sized mineral ratios in global rivers*

The F/Qtz and Pl/Qtz ratios of silt-sized sediments/SPM from global rivers demonstrate negligible correlations with MAT and MAP ($R^2 < 0.3$, Fig. 4). The correlation between the silt-sized mineral composition of global river sediments and climate is significantly different from the results observed in the sediments of East Asian rivers. This phenomenon shows that weathering has a minor influence on the composition of silt-sized minerals in global sediments with complex geological

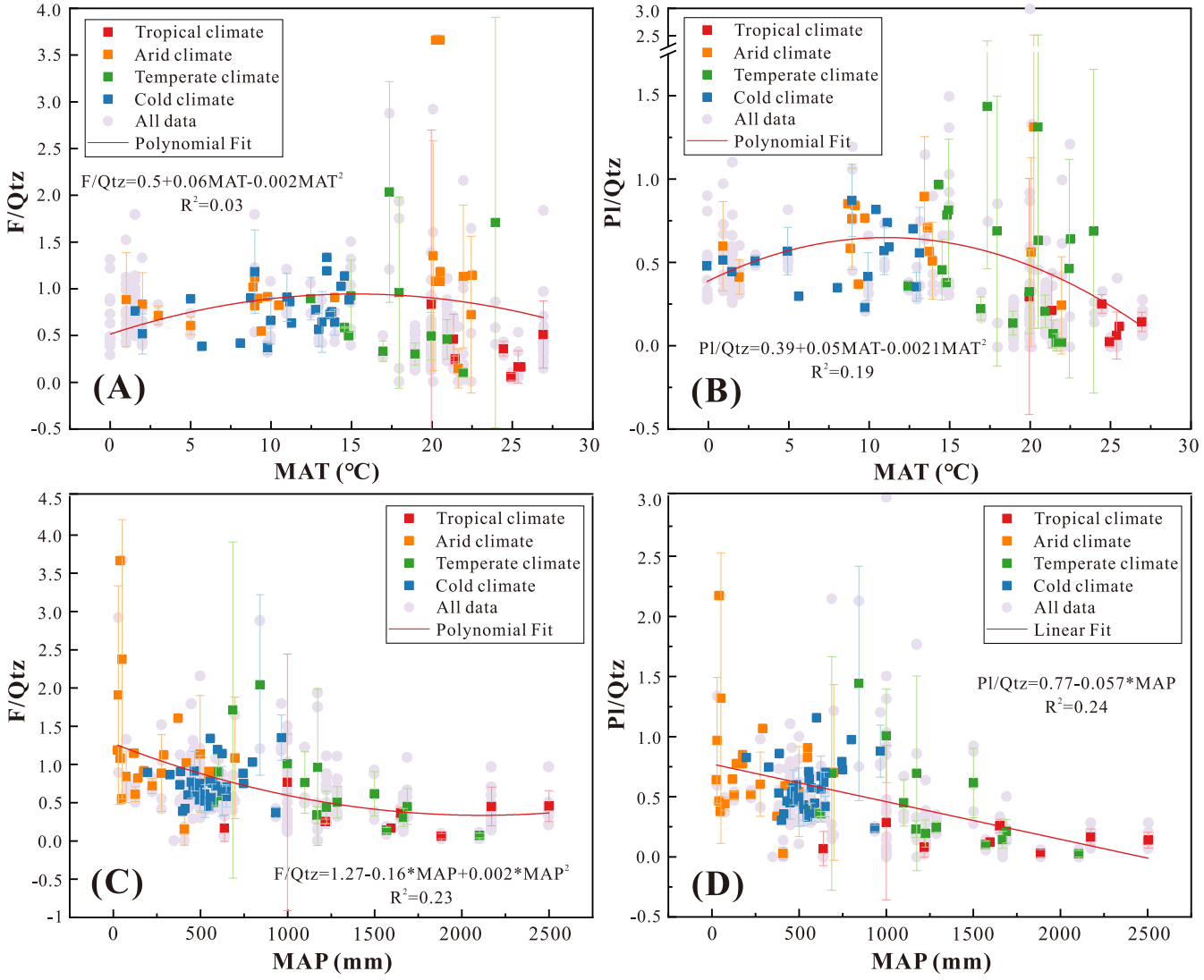

Fig. 4. Correlations between mineral composition (F/Qtz and Pl/Qtz ratios) and mean annual temperature (MAT) and precipitation (MAP) for fine-grained global river sediments (silt-sized component) and suspended particulate matter (SPM). They are divided into four climate categories, i.e., tropical (red), arid (orange), temperate (green) and cold (blue) climates, based on the Köppen-Geiger climate classification (Peel et al., 2007). All the data are represented by light purple dots, and the means and error bars are displayed for each specific temperature or precipitation value. Data fitting is mainly based on the mean values. (For interpretation of the references to colour in this figure legend, the reader is referred to the web version of this article.)

backgrounds.

The Qtz-Pl-Kfs ternary diagram data from silts of global and East Asian rivers indicate that sediments from tropical and temperate regions are closer to the quartz end-member, while those from cold and arid regions are more proximate to the feldspar end-members (Fig. 5, Fig. S5). To delve into the differences between global and regional data, we utilized the Support Vector Machine (SVM) algorithm to analyze the Qtz-Pl-Kfs dataset. SVM algorithm is a generalized linear classifier that employs supervised learning to perform binary classification (Lafdani et al., 2013). This algorithm generates an optimal dividing boundary, depicted in Fig. 5A as the SVM decision boundary (gray line), to categorize data into distinct classes (Fig. 5A). Line of Pl/Qtz = 0.3 (Fig. 5A, red line) is close to the SVM decision boundary (Fig. 5A, gray line). The classification accuracy of the SVM decision boundary and the Pl/Qtz = 0.3 line in distinguishing global samples from tropical-temperate and cold-arid climates are 89 % and 87 %, respectively (Table S4). Furthermore, the Pl/Qtz = 0.3 line can accurately distinguish samples from tropical-temperate and cold-arid climates in the 2–32 μm fraction of sediments of East Asian rivers with a 100 % accuracy, whereas the accuracy for the 32–63 μm fraction decreases to 76 % (Fig. S5). Thus, the diverse parent rock lithology and the internal grain size effects within silty sediments exert a significant influence on the silt-sized mineral composition of global river sediments, with chemical weathering having a comparatively minor impact.

4.1.3. Comparison of weathering signals in sediments of global and East Asian rivers

The high correlation coefficient R^2 ranging from 0.48 to 0.82 (Fig. 3) suggests a strong relationship between the F/Qtz (Pl/Qtz) ratios and climatic conditions in sediments of East Asian rivers. Whereas, the low correlation coefficient between F/Qtz (Pl/Qtz) and climate factors ($R^2 <$ 0.3, Fig. 4) implies a weaker link between these mineral ratios and climate in global river sediments. Similarly, the same situation occurs with the Chemical Index of Alteration (CIA). The CIA exhibits stronger correlation with MAT and MAP in the silt-sized sediments/SPM (suspended particulate matters, 4–63 μm, Shao and Yang, 2012) of East Asian rivers (R^2 = 0.86, 0.82, Li and Yang, 2010) compared to global rivers. The compiled CIA values of fine-grained sediments from global modern rivers (Deng et al., 2022) display negligible correlations with MAT (R^2 = 0.35) and MAP (R^2 = 0.1) (Fig. S6). Previous studies have indicated that CIA value is primarily controlled by mineral composition (Fu et al., 2023). Consequently, the observed pattern in CIA is largely due to differences in the correlation between mineral composition and climatic factors. There are numerous reasons that could account for the reasonable weak coupling observed between the silt-sized mineral composition of global river sediments and climate, such as the multiplicity of influencing factors, the undifferentiated grain sizes within the silty sediments (2–32 μm or 32–63 μm), and disparities in XRD mineral content analysis methods (Ali et al., 2022). However, the strong coupling between the silt-sized mineral composition of sediments in East Asian rivers and climate requires further explanations.

Asian drainages are mainly covered by sedimentary rocks/sediments (74.1 %), followed by metamorphic rocks (6.9 %) and acid plutonic rocks (7.2 %) (Hartmann and Moosdorf, 2012). The parent rock lithology of East Asian rivers involved in this study are mainly sedimentary rocks, granitoid rocks and metamorphic rocks (Lu et al., 2012; Xiao et al., 2012; Zhao et al., 2015; Shao et al., 2016; Wang et al., 2019; Qin et al., 2021; Cheng et al., 2021; Zhang et al., 2021; Yang et al., 2022). In East Asian rivers, the parent rock lithology of the sediments is mainly felsic and exhibits low heterogeneity. Consequently, climatic factors rather than parent rock lithology have a more substantial influence on shaping the mineral composition of these sediments. East Asian rivers are situated in a typical monsoonal climate zone, with the study region displaying a pronounced climatic gradient that transitions from south to north across latitudes (Li and Yang, 2010). This geographic positioning renders the silt-sized mineral composition of sediments in East Asian rivers exceptionally sensitive to climatic fluctuations. Thus, the F/Qtz (Pl/Qtz) ratio in sediments of East Asian rivers is strongly correlated with climatic conditions. Previous literature indicates that the Pl/Qtz ratio in fresh granitic rocks typically ranges between 0.3 and 2 (Fig.6, Nesbitt et al., 1996; Xu et al., 1999; Le Pera et al., 2001; Lee et al., 2008; Yusoff et al., 2013; Wang et al., 2018; Mei et al., 2021; Su et al., 2022). This suggests that sediments derived from felsic rocks with slight chemical weathering exhibit Pl/Qtz values closer to or exceeding 0.3, while, sediments undergone intense weathering generally exhibit Pl/Qtz ratios less than 0.3. This rationale supports the employment of a Pl/Qtz ratio of 0.3 as a preliminary classification criterion to distinguish between warm-wet and cold-arid climates, applicable to sediments of East Asian rivers with felsic origin, specifically within the 2–32 μm grain size fraction (Fig. S5).

4.2. Grain size effect on fine-grained sediment composition

The slight variation in grain size between the fine silt (2–32 μm) and coarse silt (32–63 μm) fractions results in differences in mineral composition (Fig. S5). With the exception of the Pl/Kfs ratio, the ratios of F/Qtz, Pl/Qtz, and Kfs/Qtz generally rise as particle size increases (Fig. S2). The Pl/Kfs ratio is notably higher in the 2–32 μm fraction and lower in the 32–63 μm fraction (Fig. S2). Grain size effect on sediment mineral composition is mainly achieved by hydrodynamic sorting, supply of source materials, chemical weathering and mechanical abrasion. Hence, it is essential to further investigate the factors that shape the distribution pattern of mineral composition across silt grain sizes in the sediments of East Asian rivers.

4.2.1. Hydrodynamic sorting

The grain size effect on traditional weathering indices is generally considered to be caused by differences in mineral composition due to density-size sorting resulting from changes in hydrodynamics (Fedo and Babechuk, 2023; Fu et al., 2023). Detrital grains with same settling velocity deposit together and minerals are separated by hydrodynamic sorting during sediment transport and depositional processes based on their size, shape, and density (Garzanti et al., 2010; Garzanti et al., 2011). Dense and subspherical minerals are more likely to be enriched in coarse-grained sediments, whereas less dense clay minerals and platy phyllosilicates are more commonly concentrated in fine-grained sediments (Guo et al., 2018), resulting in size-dependent compositional variability of sediments (Garzanti et al., 2008; Guo et al., 2018). This study believes that the relationship between silt-sized mineral ratios and grain size is less affected by hydrodynamic sorting, for the following reasons: (1) When comparing grain size differences between sand (63 μm–2 mm) and clay (<2 μm), silt-sized fraction exhibits a relatively constrained size range (2–63 μm), thereby minimizing the influence of hydrodynamic sorting; (2) The weathering residues we focused, namely, quartz, K-feldspar, and plagioclase possess similar densities and morphologies, rendering them less susceptible to hydrodynamic effects (Garzanti et al., 2008, 2009). Consequently, factors extrinsic to hydrodynamics exert a more pronounced impact on the size-dependent pattern of silt components.

4.2.2. Grain-size inheritance

Except for hydraulic sorting, the relationship between sediment mineral composition and grain size is also controlled by the original grain size of the sedimentary and igneous source rocks, which implying detrital particles may not have the same grain-size distribution when entering the sedimentary cycle (Stutenbecker et al., 2024). This effect manifests in the composition of the final sediments and known as grain-size inheritance (von Eynatten and Dunkl, 2012; Krippner et al., 2015; Feil et al., 2024). Grain-size inheritance is also observed in well-sorted beach sediments with favorable hydrodynamic conditions, further confirming that the grain size of minerals is influenced by the grain-size characteristics of the original materials (Feil et al., 2024; Shen et al.,

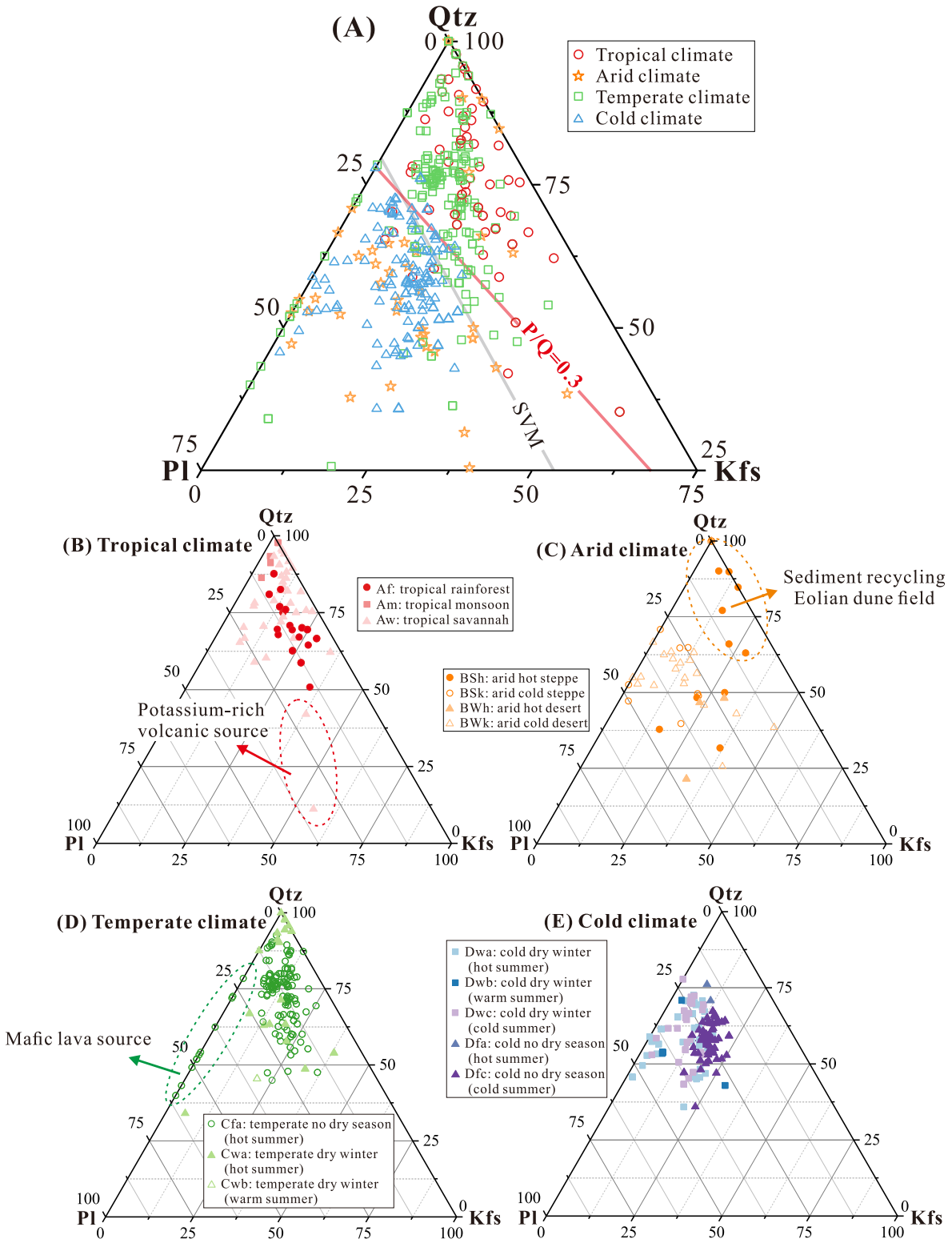

Fig. 5. Quartz-Plagioclase-K-feldspar (Qtz-Pl-Kfs) ternary diagram of silt-sized component in global fluvial sediments under four major climate zones (A), sediment samples in tropical climate zone (B), in arid climate zone (C), in temperate climate zone (D), in cold climate zone (E). Figs. 5B–5E are the enlarged versions of tropical (Af, Am, Aw), arid (BSh, BSk, BWh, BWk), temperate (Cfa, Cwa, Cwb) and cold (Dwa, Dwb, Dwc, Dfa, Dfc) climate samples from Fig. 5A, respectively. The outliers for which the mineral composition is influenced by the source rock lithology are circled in Figs. 5B–5D. The climate zones are based on the Köppen-Geiger climate classification (Peel et al., 2007). The data was divided into the training set and the testing set with a data volume of 9:1 for SVM analysis by Python 3.12.5. The decision boundary is trained by using a Linear Kernel function and obtained as $y = -1.85\times + 142$ (gray line SVM). Line of Pl/Qtz = 0.3 (red line) is close to SVM decision boundary (gray line). The accuracy of SVM decision boundary (gray line) and Pl/Qtz = 0.3 (red line) for distinguish the tropical and temperate samples from the cold and arid samples are 89 % and 87 %, respectively. The calculation method of partition accuracy is shown in Table S4. (For interpretation of the references to colour in this figure legend, the reader is referred to the web version of this article.)

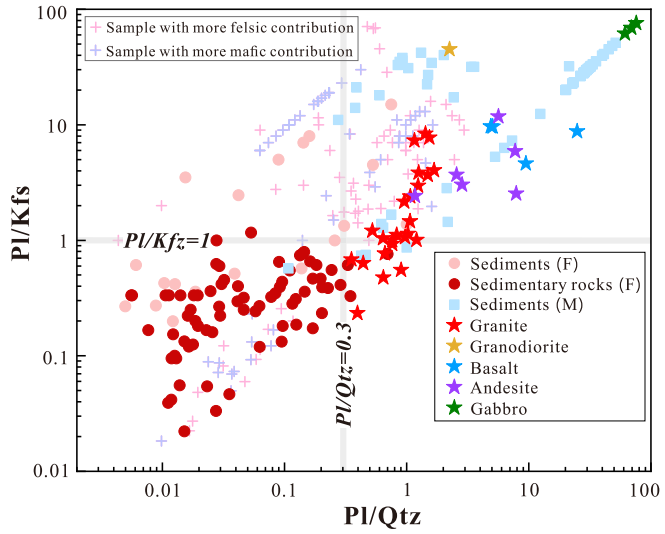

Fig. 6. Pl/Qtz versus Pl/Kfs ratios of fine-grained sediments/sedimentary rocks and fresh igneous rocks. Fresh felsic rocks include granite (red star, number = 24) and granodiorite (yellow star, n = 1), mafic rocks include basalt (blue star, n = 4), andesite (purple star, n = 7) and gabbro (green star, n = 3) (Nesbitt et al., 1996; Xu et al., 1999; Le Pera et al., 2001; Lee et al., 2008; Yusoff et al., 2013; Wang et al., 2018; Chen et al., 2020; Mei et al., 2021; Qi et al., 2022; Su et al., 2022). There are 45 modern river sediments (pink dots) and 92 sedimentary rocks (red dots) of felsic origin (Hessler and Lowe, 2006; Wani and Mondal, 2010; Etemad-Saeed et al., 2011; He et al., 2020; Kasper-Zubillaga et al., 2021), and 58 modern river sediments of mafic origin (blue squares) (Garzanti et al., 2014b, 2021; Thorpe et al., 2019; Thorpe and Hurowitz, 2020). Either the qualitative description such as felsic/mafic source or the specific parent rock type of sediments (e.g., granite or basalt) is stated in the above literatures. Mineral composition data of sedimentary rocks with mixed sources were collected and marked with crosses (Wang and Zhou, 2013; Kassi et al., 2015; Amendola et al., 2016; Corrado et al., 2019; Ji et al., 2019). Sediments of mixed sources mainly deriving from felsic rocks (as described in the literature) are represented by pink crosses, and those mainly from mafic rocks are represented by purple crosses. To facilitate the calculation and presentation of the Pl/Kfs and Pl/Qtz values, the minimum content of K-feldspar and quartz is limited to 1 %wt (i.e., 0 %wt in references is converted to 1 %wt in this study). (For interpretation of the references to colour in this figure legend, the reader is referred to the web version of this article.)

2024). Previous research has demonstrated that the grain size of sediments is influenced by the nature of their parent rocks and the source material contributions. Clay is typically derived from strongly-weathered soils or eolian sediments, whereas fine silt is often associated with the reworking of fine-grained sedimentary rocks or the soils that develop from them (Garzanti et al., 2024). Coarse silt and sand fractions result from weathering of granites and metamorphic rocks or the recycling of coarse-grained sedimentary rocks (Garzanti et al., 2024). Igneous and metamorphic rocks generate sediments with grain sizes spanning from gravel to silt (Hoskin and Sundeen, 1975). Physical abrasion of these rocks predominantly results in larger detrital particles, whereas chemical weathering further diminishes the grain size within the sediments (Roda-Boluda et al., 2018).

The lithology of river basin in East Asia involved in this study is summarized as follows. In cold climate zone, the Aihe river (AH) is characterized by a lithology predominantly consisting of granite, with a minor component of metamorphic rocks, while the lithology of Liaohe (LH) and Ziyahe rivers (ZY) are mainly sedimentary rocks (Lu et al., 2012; Qin et al., 2021). Lithology of Qinghai rivers (QH) in the arid-cold climate zone is mainly composed of sedimentary and metamorphic rocks (Xiao et al., 2012; Cheng et al., 2021; Yang et al., 2022). In the temperate climate zone, the Xijiang (XJ), Fangchengjiang (FC), and Fujian river basins (i.e., TS, JX, ML, JJ) are mostly covered by granite and sedimentary rocks (Shao et al., 2016; Zhang et al., 2021; Wang et al., 2023). The tropical Wanquanhe river (WQ) is dominated by granite and volcanic rocks, with some sedimentary rocks (Zhao et al., 2015). The major river of Yellow (HH) and Yangtze (CJ) rivers show diverse lithologies, including sedimentary, metamorphic, and igneous rocks (Wang et al., 2019). Consequently, the diversity of source rock types within river basins, ranging from initially weathered crystalline rocks to reworked sandstones and mudstones, may lead to grain-size inheritance primarily in sand-sized fractions (Garzanti et al., 2024). However, it may also exert a minor influence on the different mineral compositions of coarse silt (32–63 μm) and fine silt (2–32 μm) fractions in sediments. The specific mechanisms and extents of these influences cannot be definitively ascertained in this study.

4.2.3. Weathering and mechanical abrasion

From coarse to fine sediments, there is a general trend of increasing phyllosilicate content and decreasing quartz and feldspar abundance (von Eynatten et al., 2016). Furthermore, due to the faster weathering rate of feldspar compared to quartz, feldspar is more extensively depleted than quartz (Worthington et al., 2016). From a kinetic perspective, the dissolution rates of minerals are closely linked to the available surface area of mineral particles (Yuan et al., 2019). The BET (Brunauer-EmmettTeller) specific surface area is influenced by mineral grain size (Brantley and Mellott, 2000) and the presence of etch pits, cracks, and porosity (Schulz and White, 1999). As grain size decreases, specific surface area increases, enhancing mineral dissolution rates of quartz and feldspar (Schulz and White, 1999; Israeli and Emmanuel, 2018; Yuan et al., 2019). However, even within the same grain size range, feldspar, which has high content and highly-reactive etch pit walls (Pollet-Villard et al., 2016), exhibits a significantly greater increase in effective surface area and dissolution rate compared to quartz (less reactive etch pit) (Brantley and Mellott, 2000; Gautier et al., 2001). The discrepancy in weathering and dissolution rate between feldspar and quartz could provide a plausible explanation for the higher F/Qtz, Pl/Qtz and Kfs/Qtz ratios in the 32–63 μm fraction than that in the 2–32 μm fractions (Figs. S2, S5).

Chemical weathering of feldspar grains occurs preferentially at the surface and along cleavage and twin planes, which in turn accelerates the mechanical fracturing of the mineral grains (Berner and Holdren, 1979; Banfield and Eggleton, 1990; von Eynatten et al., 2016). The weathering rate of plagioclase is a factor of 10–10^2 times faster than that of K-feldspar (Zhu, 2005). Preferential weathering of plagioclase is conducive to its easy fracturing into small pieces, which are concentrated into fine components (16–125 μm, von Eynatten et al., 2016). The stronger chemical-physical abrasion of plagioclase over K-feldspar may explain the phenomenon of higher Pl/Kfs ratios in the 2–32 μm fraction and lower Pl/Kfs ratios in the 32–63 μm fraction (Fig. S2).

4.2.4. Climate or lithology controls on clay mineral composition?

Clay minerals in fine-grained sediments are often used to reflect climate and chemical weathering intensity (Warr et al., 2024). Kaolinite is generally considered to be formed under strong leaching and warm-wet climatic conditions, while illite and chlorite are formed in dry and cold environments (Liu et al., 2016; Warr, 2022). Chemical weathering-dominated Al-rich illite exhibits higher values of illite chemistry index than that of physical erosion-dominated Fe-Mg-rich illite (Esquevin, 1969). Thus, the higher values of Kao/(Ill+Chl) ratio and illite chemistry index indicate stronger weathering intensity (Mei et al., 2021; Wang et al., 2023).

We analyzed the kaolinite/(illite+chlorite) ratio and illite chemistry index in clay-sized fractions in sediments (<2 μm) of Qinghai and Fujian rivers, part of East Asian rivers. Results suggest that clay mineral indices can distinguish chemical weathering intensity of river sediments in Qinghai (dry and cold climate) from river sediments (TS, JX, ML, JJ) in Fujian (warm and wet climate) (Fig. S7). However, the clay mineral indices of Fujian rivers sediments do not show monotonically increasing trends with temperature and precipitation (Fig. S7). Although it has

been found that the Kao/(Ill+Chl) ratio and illite chemistry index show parabolic changes with precipitation (Lyu and Lu, 2024; Wang, 2024) with change threshold of 1800–2000 mm. The irregular data of clay mineral compositions in sediments (Fig. 4, Fig. S7) were caused by the lithology of the parent rocks. The sediments in the Jiaoxi (JX) and Tongshanxi (TS) basins receive a greater material supply from recycled sedimentary rocks, with higher illite content and lower illite chemistry index (Wang, 2024). Therefore, integrating the aforementioned research on silt-grade components, we believe that source material supply and weathering have pronounced influences on the mineral composition of fine-grained sediments and their correlations with grain size.

4.3. Lithological effects on sediment silt-sized mineral composition

Global river sediment samples reveal lithological complexities and significant influences on silt-sized mineral ratios. The heterogeneity of global river lithology will enhance the lithology signal and weaken the climate signal. Some samples deviate significantly from the range constrained by most of the samples belonging to the same climatic zone, such as tropical Rwanda sediments (Fig. 5B) derived from potassic-ultrapotassic lavas (e.g., basanite, mugearite, trachybasalt) (Garzanti et al., 2015), temperate Uruguay sediments (Fig. 5D) supplied by mafic lavas and sedimentary strata (Garzanti et al., 2021), the quartz-rich arid Okavango sediments (Fig. 5C) received lots of recycled and eolian materials (Garzanti et al., 2014a). Two samples of river sediments in East Asia, 20WQ-2 derived from feldspathic quartz sandstone and granite (Zhao et al., 2015) and 20AH-1 sourced from monzonitic granite and granodiorite, are characterized with abnormally high F/Qtz and Pl/Qtz ratios (Fig. 3). These phenomena urge us to further understand the influence of lithology on silt-sized mineral ratios.

4.3.1. Felsic and mafic source rocks

We collected mineral composition data of fresh igneous rocks, felsic- and mafic-sourced fine-grained sediments and sedimentary rocks, as shown in Fig. 6. Rocks with different proportions of mafic and felsic minerals are not equally vulnerable to weathering. Mafic rocks are more susceptible to weathering with high weathering rates (Worthington et al., 2016), and within these rocks, plagioclase is more prevalent than K-feldspar (Spalletti et al., 2008; Thorpe and Hurowitz, 2020). For example, fresh mafic rocks, including basalt, andesite, and gabbro, typically exhibit a Pl/Kfs ratio greater than 2 and a Pl/Qtz ratio above 1 (Fig. 6). In contrast, granite shows a Pl/Kfs ratio ranging from 0.2 to 10 and a Pl/Qtz ratio between 0.3 and 2 (Fig. 6). Even in different climatic zones and subjected to varying degrees of chemical weathering, the initial mineral composition characteristics of the parent rocks can still be preserved in fine-grained sediments to some extent. Fine-grained sediments originated from mafic rocks have higher Pl/Qtz (>0.3) and Pl/Kfs (>1) ratio than those in sediments/sedimentary rocks originated from felsic rocks (Pl/Qtz <0.3 and Pl/Kfs <1) (Fig. 6). Several mixed source samples with high mafic contributions (plagioclase-rich) are located in the region where Pl/Qtz < 0.3 and Pl/Kfs < 1, likely indicate strong weathering alteration and intense plagioclase decomposition (Kamp, 2010; Su et al., 2022).

Among felsic rocks, monzogranites, granodiorites, and diorites are characterized by a predominance of plagioclase over K-feldspar, resulting in relatively high Pl/Kfs ratios (ca. 50 in Fig. 6; Hussain et al., 2004; Caracciolo et al., 2012; Boocock et al., 2023). Sediments from these rocks exhibit higher F/Qtz and Pl/Qtz ratios than those from granites (von Eynatten et al., 2012). Thus, there are still some sediments sourced from felsic rocks, as well as samples with a predominant felsic parent rocks in mixed-source sediments (pink cross) fall in the area where Pl/Kfs > 1 (Fig. 6), which emphasized that the internal transformation of felsic rocks can also cause great changes in the mineral composition of sediments, especially for sedimentary strata study. The above provides a reasonable explanation for the anomalous high F/Qtz and Pl/Qtz ratios of samples 20WQ-2 and 20AH-1 derived from felsic rocks. Overall, the F/Qtz and P/Qtz ratios are highly influenced by source rock lithologies.

4.3.2. Sediment recycling

Apart from igneous rocks, sedimentary rocks and metamorphic rocks cover the majority of the Earth's land surface (ca. 80 %, Peucker-Ehrenbrink and Miller, 2004; Hartmann and Moosdorf, 2012) and should be considered as important parent rock types of the drainage basins. The record in sedimentary rocks may reflect either first-cycle or multi-cycle weathering intensity signals (Guo et al., 2018). The failed application of silt-sized F/Qtz and Pl/Qtz ratios to evaluate weathering intensity of sediments derived from sedimentary rocks is primarily attributed to sediment recycling. Sediment recycling occurs extensively in a variety of tectonic settings, including stable cratons, rifted margins, arc-trench systems and orogenic belts, particularly in subduction complexes (Garzanti et al., 2013c). Quartz is stably resistant to weathering and concentrate in polycyclic sedimentary-metasedimentary rocks during recycling (Guo et al., 2018), resulting in very low Pl/Qtz values in the silt-sized fraction of current-cycled sediments, e.g., the arid Okavango river sediments (Fig. 5C, Garzanti et al., 2022), which may lead to an overestimation of weathering intensity in arid desert or temperate coastal areas (Fig. 5A).

Geochemical and petrological methods have been proposed to determine whether a sample has undergone significant sedimentary recycling through the compositional and textural analysis. The plot of quartz-sensitive WIP (Weathering Index of Parker) and quartz-insensitive CIA can qualitatively distinguish first-cycled sediments from multi-cycled sediments (Parker, 1970; Garzanti et al., 2013a, 2013b). Guo et al. (2024) introduced the chemical index of quartz-enrichment (CIQ) index to quantitatively assess the extent of quartz enrichment by combining the CIA/WIP diagram. Furthermore, the Mafic-Felsic-Weathering (MFW) ternary diagram (Xie et al., 2018), the Index of Compositional Variability (ICV) (Cox et al., 1995) and the discriminant function diagram (Roser and Korsch, 1988) are available for identifying sedimentary recycling (Li et al., 2023). Compositional and textural analysis of polycyclic sandstones (63 μm–0.5 mm) commonly show high content of lithic fragments of sedimentary-metasedimentary rocks (Garzanti et al., 2013c) and/or a prevalence of rounded to subrounded monocrystalline quartz (Corcoran, 2005; Garzanti et al., 2022). The textural characteristics of fine-grained sediments can be observed using smear slide petrography (Phillips and Littler, 2022). Results of smear slide petrography has shown that the roundness of quartz in the silt-sized component (32–63 μm) of Taiwan river sediments dominated by sedimentary rocks and metasedimentary rocks is rounder than that in sediments from of Fujian rivers dominated by granites (Fig. S8). Utilizing the aforementioned methods to identify sedimentary recycling help to accurately interpret the provenance, recycling, and weathering signals in the silt-sized mineral composition of river sediments.

5. Conclusions

In this contribution, we analyzed and compared the silt-sized mineral composition in sediments from East Asian rivers with those from global rivers. Strong correlations were identified between the silt-sized mineral ratios (i.e., Pl/Qtz, F/Qtz) in river sediments of East Asia and climatic factors. Notably, the Pl/Qtz ratio of the 2–32 μm fraction demonstrated significant qualitative correlations with MAT ($R^2 = 0.75$) and MAP ($R^2 = 0.82$), with a Pl/Qtz ratio of 0.3 effectively differentiating warm-humid climates from dry-cold climates. However, the close link between silt mineral composition and climate observed in East Asian rivers is not as pronounced in global river sediments, which generally exhibit a weak correlation.

This phenomenon underscores the multiple and complex controls on silt-sized mineral composition, such as parent rock lithology, sediment recycling, climate-driven weathering and grain size effects. The

increased contribution of plagioclase from intermediate-mafic rocks and the enrichment of recycled quartz can affect the composition of fine-grained sediments, preventing the silt-sized mineral ratios as independent and universally applicable weathering indices. If used as weathering indices, silt-sized Pl/Qtz and F/Qtz ratios are most effective for river sediments or sedimentary rocks with stable provenance, felsic parent rocks and minimal sediment recycling. Despite the narrow size range of silt, there are compositional differences between the 2–32 μm and 32–63 μm fractions that are not attributed to hydrodynamic sorting but are primarily due to chemical-physical abrasion and grain size inheritance from parent rocks. This study highlights the influence of geological controls on sediment silt-sized mineral composition and underscores the importance of grain size differentiation and multi-grain size mineral composition analysis of sediments in reducing biases in weathering and provenance analysis.

CRediT authorship contribution statement

Hanjing Fu: Writing – original draft, Methodology, Conceptualization. **Xing Jian:** Writing – original draft, Supervision, Funding acquisition, Conceptualization. **Zhihua Zhang:** Methodology, Investigation. **Hanqing Pan:** Methodology, Data curation.

Declaration of competing interest

We declare that we don't have any conflict of interest.

Data availability

I have share data in supplemental materials

Acknowledgments

This study was funded by the National Natural Science Foundation of China (Nos. 42476051, 41806052) and the Natural Science Foundation of Xiamen, China (No. 3502Z20227006). The climatic data of East Asia river samples are from "National Earth System Science Data Center, National Science & Technology Infrastructure of China. (http://www.geodata.cn)". We thank Lihui Wang for her help with lab analysis, Hanghai Liang, Shuo Zhang, Dongming Hong, Haowei Mei for their help with sampling. We appreciate the constructive comments from Dr. Eduardo Garzanti, Dr. Juan Kasper-Zubillaga and other reviewers.

Appendix A. Supplementary data

Supplementary data to this article can be found online at https://doi.org/10.1016/j.palaeo.2024.112700.

References

Adriaens, R., Zeelmaekers, E., Fettweis, M., Vanlierde, E., Vanlede, J., Stassen, P., Elsen, J., Środoń, J., Vandenberghe, N., 2018. Quantitative clay mineralogy as provenance indicator for recent muds in the southern North Sea. Mar. Geol. 398, 48–58. https://doi.org/10.1016/j.margeo.2017.12.011.

Ali, A., Chiang, Y.W., Santos, R.M., 2022. X-ray diffraction techniques for mineral characterization: a review for engineers of the fundamentals, applications, and research directions. Minerals 12 (2), 205. https://doi.org/10.3390/min12020205.

Alizai, A., Hillier, S., Clift, P.D., Giosan, L., Hurst, A., VanLaningham, S., Macklin, M., 2012. Clay mineral variations in Holocene terrestrial sediments from the Indus Basin. Quat. Res. 77 (3), 368–381. https://doi.org/10.1016/j.yqres.2012.01.008.

Amendola, U., Perri, F., Critelli, S., Monaco, P., Cirilli, S., Trecci, T., Rettori, R., 2016. Composition and provenance of the Macigno formation (late Oligocene–early Miocene) in the Trasimeno lake area (northern Apennines). Mar. Pet. Geol. 69, 146–167. https://doi.org/10.1016/j.marpetgeo.2015.10.019.

Andò, S., Garzanti, E., Padoan, M., Limonta, M., 2012. Corrosion of heavy minerals during weathering and diagenesis: a catalog for optical analysis. Sediment. Geol. 280, 165–178. https://doi.org/10.1016/j.sedgeo.2012.03.023.

Assallay, A.M., Rogers, C.D.F., Smalley, I.J., Jefferson, I.F., 1998. Silt: 2–62 μm, 9–4φ. Earth Sci. Rev. 45 (1–2), 61–88. https://doi.org/10.1016/s0012-8252(98)00035-x.

Banfield, J.F., Eggleton, R.A., 1990. Analytical transmission electron microscope studies of plagioclase, muscovite, and K-feldspar weathering. Clay Clay Miner. 38, 77–89. https://doi.org/10.1346/CCMN.1990.0380111.

Berner, R.A., Holdren Jr., G.R., 1979. Mechanism of feldspar weathering—II. Observations of feldspars from soils. Geochimica et Cosmochimica Acta 43 (8), 1173–1186.

Bhuiyan, M.A.H., Rahman, M.J.J., Dampare, S.B., Suzuki, S., 2011. Provenance, tectonics and source weathering of modern fluvial sediments of the Brahmaputra–Jamuna River, Bangladesh: Inference from geochemistry. J. Geochem. Explor. 111 (3), 113–137. https://doi.org/10.1016/j.gexplo.2011.06.008.

Bista, D., Kienast, S.S., Hill, P.S., Kienast, M., 2016. Sediment sorting and focusing in the eastern equatorial Pacific. Mar. Geol. 382, 151–161. https://doi.org/10.1016/j.margeo.2016.09.016.

Blott, S.J., Pye, K., 2012. Particle size scales and classification of sediment types based on particle size distributions: Review and recommended procedures. Sedimentology 59 (7), 2071–2096. https://doi.org/10.1111/j.1365-3091.2012.01335.

Boocock, T.J., Stüeken, E.E., Bybee, G.M., König, R., Boyce, A.J., Prytulak, J., Buisman, I., Mikhail, S., 2023. Equilibrium partitioning and isotopic fractionation of nitrogen between biotite, plagioclase, and K-feldspar during magmatic differentiation. Geochim. Cosmochim. Acta 356, 116–128. https://doi.org/10.1016/j.gca.2023.07.010.

Borromeo, L., Andò, S., France-Lanord, C., Coletti, G., Hahn, A., Garzanti, E., 2019. Provenance of Bengal shelf sediments: 1. Mineralogy and geochemistry of silt. Minerals 9 (10), 640. https://doi.org/10.3390/min9100640.

Bouchez, J., Gaillardet, J., France-Lanord, C., Maurice, L., Dutra-Maia, P., 2011. Grain size control of river suspended sediment geochemistry: Clues from Amazon River depth profiles. Geochem. Geophys. Geosyst. 12 (3). https://doi.org/10.1029/2010GC003380.

Brahim, M., Abdelfattah, A., Sammari, C., Aleya, L., 2015. Surface sediment dynamics along with hydrodynamics along the shores of Tunis Gulf (North-Eastern Mediterranean). J. Afr. Earth Sci. 103, 30–41. https://doi.org/10.1016/j.jafrearsci.2014.11.014.

Brantley, S.L., Mellott, N.P., 2000. Surface area and porosity of primary silicate minerals. Am. Mineral 85 (11−12), 1767–1783. https://doi.org/10.2138/am-2000-11-1220.

Brantley, S.L., Shaughnessy, A., Lebedeva, M.I., Balashov, V.N., 2023. How temperature-dependent silicate weathering acts as Earth's geological thermostat. Science 379 (6630), 382–389. https://doi.org/10.1126/science.add2922.

Caracciolo, L., Tolosana-Delgado, R., Le Pera, E., von Eynatten, H., Arribas, J., Tarquini, S., 2012. Influence of granitoid textural parameters on sediment composition: implications for sediment generation. Sediment. Geol. 280, 93–107. https://doi.org/10.1016/j.sedgeo.2012.07.005.

Chen, X., Zhang, Y., Huo, H., Wu, Z., 2020. Study of high tensile strength of natural continuous basalt fibers. J. Nat. Fibers 17 (2), 214–222. https://doi.org/10.1080/15440478.2018.1477087.

Cheng, F., Jolivet, M., Guo, Z., Wang, L., Zhang, C., Li, X., 2021. Cenozoic evolution of the Qaidam basin and implications for the growth of the northern Tibetan plateau: a review. Earth Sci. Rev. 220, 103730. https://doi.org/10.1016/j.earscirev.2021.103730.

Corcoran, P.L., 2005. Recycling and chemical weathering in tectonically controlled Mesozoic-Cenozoic basins of New Zealand. Sedimentology 52 (4), 757–774. https://doi.org/10.1111/j.1365-3091.2005.00723.x.

Corrado, S., Aldega, L., Perri, F., Critelli, S., Muto, F., Schito, A., Tripodi, V., 2019. Detecting syn-orogenic extension and sediment provenance of the Cilento wedge top basin (southern Apennines, Italy): Mineralogy and geochemistry of fine-grained sediments and petrography of dispersed organic matter. Tectonophysics 750, 404–418. https://doi.org/10.1016/j.tecto.2018.10.027.

Cox, R., Lowe, D.R., Cullers, R.L., 1995. The influence of sediment recycling and basement composition on evolution of mudrock chemistry in the southwestern United States. Geochim. Cosmochim. Acta 59 (14), 2919–2940. https://doi.org/10.1016/0016-7037(95)00185-9.

Dekov, V.M., Komy, Z., Araujo, F., Van Put, A., Van Grieken, R., 1997. Chemical composition of sediments, suspended matter, river water and ground water of the Nile (Aswan-Sohag traverse). Sci. Total Environ. 201 (3), 195–210. https://doi.org/10.1016/S0048-9697(97)84057-0.

Deng, K., Yang, S., Guo, Y., 2022. A global temperature control of silicate weathering intensity. Nat. Commun. 13 (1), 1781. https://doi.org/10.1038/s41467-022-29415-0.

Ding, T.P., Gao, J.F., Tian, S.H., Wang, H.B., Li, M., 2011. Silicon isotopic composition of dissolved silicon and suspended particulate matter in the Yellow River, China, with implications for the global silicon cycle. Geochim. Cosmochim. Acta 75 (21), 6672–6689. https://doi.org/10.1016/j.gca.2011.07.040.

Dinis, P.A., Garzanti, E., Hahn, A., Vermeesch, P., Cabral-Pinto, M., 2020. Weathering indices as climate proxies. A step forward based on Congo and SW African river muds. Earth Sci. Rev. 201, 103039. https://doi.org/10.1016/j.earscirev.2019.103039.

Esquevin, J., 1969. Influence de la composition chimique des illites sur leur cristallinit`e. Bull. Centre Rech. Pau-SNPA 3 (1), 147–153.

Etemad-Saeed, N.A., Hosseini-Barzi, M.A., Armstrong-Altrin, J.S., 2011. Petrography and geochemistry of clastic sedimentary rocks as evidences for provenance of the lower Cambrian Lalun Formation, Posht-e-badam block, Central Iran. J. Afr. Earth Sci. 61 (2), 142–159. https://doi.org/10.1016/j.jafrearsci.2011.06.003.

von Eynatten, H., Dunkl, I., 2012. Assessing the sediment factory: the role of single grain analysis. Earth Sci. Rev. 115 (1–2), 97–120. https://doi.org/10.1016/j.earscirev.2012.08.001.

von Eynatten, H., Tolosana-Delgado, R., Karius, V., 2012. Sediment generation in modern glacial settings: Grain-size and source-rock control on sediment

composition. Sediment. Geol. 280, 80–92. https://doi.org/10.1016/j.sedgeo.2012.03.008.
von Eynatten, H., Tolosana-Delgado, R., Karius, V., Bachmann, K., Caracciolo, L., 2016. Sediment generation in humid Mediterranean setting: Grain-size and source-rock control on sediment geochemistry and mineralogy (Sila Massif, Calabria). Sediment. Geol. 336, 68–80. https://doi.org/10.1016/j.sedgeo.2015.10.008.
Fedo, C.M., Nesbitt, H.W., Young, G.M., 1995. Unraveling the effects of potassium metasomatism in sedimentary rocks and paleosols, with implications for paleoweathering conditions and provenance. Geology 23 (10), 921–924. https://doi.org/10.1130/0091-7613(1995)023<0921:UTEOPM>2.3.CO;2.
Fedo, C.M., Babechuk, M.G., 2023. Petrogenesis of siliciclastic sediments and sedimentary rocks explored in three-dimensional Al2O3–CaO*+ Na2O–K2O–FeO+ MgO (A–CN–K–FM) compositional space. Canadian Journal of Earth Sciences 60 (7), 818–838. https://doi.org/10.1139/cjes-2022-0051.
Feil, S., von Eynatten, H., Dunkl, I., Schönig, J., Lünsdorf, N.K., 2024. Inherited grain-size distributions: effect on heavy-mineral assemblages in modern and ancient sediments. J. Geophys. Res. Earth 129 (2), e2023JF007356. https://doi.org/10.1029/2023JF007356.
Franco-Fraguas, P., Burone, L., Mahiques, M., Ortega, L., Urien, C., Muñoz, A., López, G., Marin, Y., Carranza, A., Lahuerta, N., de Mello, C., 2014. Hydrodynamic and geomorphological controls on surface sedimentation at the subtropical shelf front/Brazil–Malvinas confluence transition off Uruguay (southwestern Atlantic continental margin). Mar. Geol. 349, 24–36. https://doi.org/10.1016/j.margeo.2013.12.010.
Frings, P.J., Buss, H.L., 2019. The central role of weathering in the geosciences. Elements: Intern. Magaz. Mineral. Geochem. Petrol. 15 (4), 229–234. https://doi.org/10.2138/gselements.15.4.229.
Fu, H., Jian, X., Liang, H., Zhang, W., Shen, X., Wang, L., 2022. Tectonic and climatic forcing of chemical weathering intensity in the northeastern Tibetan Plateau since the middle Miocene. Catena 208, 105785. https://doi.org/10.1016/j.catena.2021.105785.
Fu, H., Jian, X., Pan, H., 2023. Bias in sediment chemical weathering intensity evaluation: a numerical simulation study. Earth Sci. Rev., 104574 https://doi.org/10.1016/j.earscirev.2023.104574.
Gaillardet, J., Dupré, B., Allègre, C.J., 1999. Geochemistry of large river suspended sediments: silicate weathering or recycling tracer? Geochim. Cosmochim. Acta 63 (23–24), 4037–4051. https://doi.org/10.1016/S0016-7037(99)00307-5.
Garzanti, E., Andò, S., Vezzoli, G., 2008. Settling equivalence of detrital minerals and grain-size dependence of sediment composition. Earth Planet. Sci. Lett. 273 (1–2), 138–151. https://doi.org/10.1016/j.epsl.2008.06.020.
Garzanti, E., Andò, S., Vezzoli, G., 2009. Grain-size dependence of sediment composition and environmental bias in provenance studies. Earth Planet. Sci. Lett. 277 (3–4), 422–432. https://doi.org/10.1016/j.epsl.2008.11.007.
Garzanti, E., Andò, S., France-Lanord, C., Vezzoli, G., Censi, P., Galy, V., Najman, Y., 2010. Mineralogical and chemical variability of fluvial sediments: 1. Bedload sand (Ganga–Brahmaputra, Bangladesh). Earth and Planetary Science Letters 299 (3-4), 368–381. https://doi.org/10.1016/j.epsl.2010.09.017.
Garzanti, E., Andó, S., France-Lanord, C., Censi, P., Vignola, P., Galy, V., Lupker, M., 2011. Mineralogical and chemical variability of fluvial sediments 2. Suspended-load silt (Ganga–Brahmaputra, Bangladesh). Earth Planet. Sci. Lett. 302 (1–2), 107–120. https://doi.org/10.1016/j.epsl.2010.11.043.
Garzanti, E., Padoan, M., Andò, S., Resentini, A., Vezzoli, G., Lustrino, M., 2013a. Weathering and relative durability of detrital minerals in equatorial climate: sand petrology and geochemistry in the East African Rift. J. Geol. 121 (6), 547–580. https://doi.org/10.1086/673259.
Garzanti, E., Padoan, M., Setti, M., Najman, Y., Peruta, L., Villa, I.M., 2013b. Weathering geochemistry and Sr-Nd fingerprints of equatorial upper Nile and Congo muds. Geochem. Geophys. Geosyst. 14 (2), 292–316. https://doi.org/10.1002/ggge.20060.
Garzanti, E., Limonta, M., Resentini, A., Bandopadhyay, P.C., Najman, Y., Andò, S., Vezzoli, G., 2013c. Sediment recycling at convergent plate margins (Indo-Burman ranges and Andaman–Nicobar Ridge). Earth Sci. Rev. 123, 113–132. https://doi.org/10.1016/j.earscirev.2013.04.008.
Garzanti, E., Vermeesch, P., Padoan, M., Resentini, A., Vezzoli, G., Andò, S., 2014a. Provenance of passive-margin sand (Southern Africa). J. Geol. 122 (1), 17–42. https://doi.org/10.1086/674803.
Garzanti, E., Padoan, M., Setti, M., López-Galindo, A., Villa, I.M., 2014b. Provenance versus weathering control on the composition of tropical river mud (southern Africa). Chem. Geol. 366, 61–74. https://doi.org/10.1016/j.chemgeo.2013.12.016.
Garzanti, E., Andò, S., Padoan, M., Vezzoli, G., El Kammar, A., 2015. The modern Nile sediment system: processes and products. Quat. Sci. Rev. 130, 9–56. https://doi.org/10.1016/j.quascirev.2015.07.011.
Garzanti, E., Dinis, P., Vezzoli, G., Borromeo, L., 2021. Sand and mud generation from continental flood basalts in contrasting landscapes and climatic conditions (Paraná–Etendeka conjugate igneous provinces, Uruguay and Namibia). Sedimentology 68 (7), 3447–3475. https://doi.org/10.1111/sed.12905.
Garzanti, E., Pastore, G., Stone, A., Vainer, S., Vermeesch, P., Resentini, A., 2022. Provenance of Kalahari Sand: paleoweathering and recycling in a linked fluvial-aeolian system. Earth Sci. Rev. 224, 103867. https://doi.org/10.1016/j.earscirev.2021.103867.
Garzanti, E., Bayon, G., Barbarano, M., Resentini, A., Vezzoli, G., Pastore, G., Adeaga, O., 2024. Anatomy of Niger and Benue river sediments from clay to granule: grain-size dependence and provenance budgets, Nigeria. Journal of Sedimentary Research 94 (5), 714–735. https://doi.org/10.2110/jsr.2024.024.
Gautier, J.M., Oelkers, E.H., Schott, J., 2001. Are quartz dissolution rates proportional to BET surface areas? Geochim. Cosmochim. Acta 65 (7), 1059–1070. https://doi.org/10.1016/S0016-7037(00)00570-6.
Goodfellow, B.W., 2012. A granulometry and secondary mineral fingerprint of chemical weathering in periglacial landscapes and its application to blockfield origins. Quat. Sci. Rev. 57, 121–135. https://doi.org/10.1016/j.quascirev.2012.09.023.
Gordeev, V.V., Dara, O.M., Filippov, A.S., Belorukov, S.K., Lokhov, A.S., Kotova, E.I., Kochenkova, A.I., 2022. Mineralogy of Particulate Suspended Matter of the Severnaya Dvina River (White Sea, Russia). Minerals 12 (12), 1600. https://doi.org/10.3390/min12121600.
Gou, L.F., Huang, F., Yang, S.Y., Wei, G.J., Zhao, Z.Q., Jin, Z.D., 2024. Cation isotopes trace chemical weathering. Fund. Res. https://doi.org/10.1016/j.fmre.2023.12.005 (In Press).
Guo, Y., Yang, S., Su, N., Li, C., Yin, P., Wang, Z., 2018. Revisiting the effects of hydrodynamic sorting and sedimentary recycling on chemical weathering indices. Geochim. Cosmochim. Acta 227, 48–63.
Guo, Y., Yang, S., Deng, K., 2021. Disentangle the hydrodynamic sorting and lithology effects on sediment weathering signals. Chem. Geol. 586, 120607. https://doi.org/10.1016/j.chemgeo.2021.120607.
Guo, Y., Li, Y., Deng, K., Wang, Z., Yang, S., 2024. Decoding the signals of sediment weathering: toward a quantitative approach. Chem. Geol. 651, 122009. https://doi.org/10.1016/j.chemgeo.2024.122009.
Gutiérrez-Pastor, J., Nelson, C.H., Goldfinger, C., Escutia, C., 2013. Sedimentology of seismo-turbidites off the Cascadia and northern California active tectonic continental margins, Northwest Pacific Ocean. Mar. Geol. 336, 99–119. https://doi.org/10.1016/j.margeo.2012.11.010.
Hamann, Y., Ehrmann, W., Schmiedl, G., Krüger, S., Stuut, J.B., Kuhnt, T., 2008. Sedimentation processes in the Eastern Mediterranean Sea during the late Glacial and Holocene revealed by end-member modelling of the terrigenous fraction in marine sediments. Mar. Geol. 248 (1–2), 97–114. https://doi.org/10.1016/j.margeo.2007.10.009.
Harnois, L., 1988. The CIW index: a new chemical index of weathering. Sediment. Geol. 55 (3), 319–322. https://doi.org/10.1016/0037-0738(88)90137-6.
Hartmann, J., Moosdorf, N., 2012. The new global lithological map database GLiM: A representation of rock properties at the Earth surface. Geochemistry, Geophysics, Geosystems 13 (12). https://doi.org/10.1029/2012GC004370.
He, J., Garzanti, E., Dinis, P., Yang, S., Wang, H., 2020. Provenance versus weathering control on sediment composition in tropical monsoonal climate (South China)-1. Geochemistry and clay mineralogy. Chem. Geol. 558, 119860. https://doi.org/10.1016/j.chemgeo.2020.119860.
Hessler, A.M., Lowe, D.R., 2006. Weathering and sediment generation in the Archean: an integrated study of the evolution of siliciclastic sedimentary rocks of the 3.2 Ga Moodies Group, Barberton Greenstone Belt, South Africa. Precambrian Res. 151 (3–4), 185–210. https://doi.org/10.1016/j.precamres.2006.08.008.
Hessler, A.M., Zhang, J., Covault, J., Ambrose, W., 2017. Continental weathering coupled to Paleogene climate changes in North America. Geology 45 (10), 911–914. https://doi.org/10.1130/G39245.1.
Hillier, S., 2000. Accurate quantitative analysis of clay and other minerals in sandstones by XRD: comparison of a Rietveld and a reference intensity ratio (RIR) method and the importance of sample preparation. Clay Miner. 35 (1), 291–302. https://doi.org/10.1180/000985500546666.
Hilton, R.G., 2023. Earth's persistent thermostat. Science 379 (6630), 329–330. https://doi.org/10.1126/science.adf3379.
Hoskin, C.M., Sundeen, D.A., 1975. Relationship between grain size of source rock and derived sediment, Biorka Island tonalite, southeastern Alaska. The Journal of Geology 83 (5), 567–578. https://doi.org/10.1086/628141.
Hou, C., Yi, Y., Song, J., Zhou, Y., 2021. Effect of water-sediment regulation operation on sediment grain size and nutrient content in the lower Yellow River. J. Clean. Prod. 279, 123533. https://doi.org/10.1016/j.jclepro.2020.123533.
Hu, C., Tian, Y., Liu, X., Jia, Y., 2024. Permeability of surface clay-bearing sediments in Shenhu Area of South China Sea. Eng. Geol., 107535 https://doi.org/10.1016/j.enggeo.2024.107535.
Huang, J., Jiao, W., Liu, J., Wan, S., Xiong, Z., Zhang, J., Yang, Z.B., Li, A., Li, T., 2021. Sediment distribution and dispersal in the southern South China Sea: evidence from clay minerals and magnetic properties. Mar. Geol. 439, 106560. https://doi.org/10.1016/j.margeo.2021.106560.
Hussain, M.F., Mondal, M.E.A., Ahmad, T., 2004. Petrological and geochemical characteristics of Archean gneisses and granitoids from Bastar craton, Central India–implication for subduction related magmatism. Gondwana Res. 7 (2), 531–537. https://doi.org/10.1016/S1342-937X(05)70803-0.
Ingersoll, R.V., Bullard, T.F., Ford, R.L., Grimm, J.P., Pickle, J.D., Sares, S.W., 1984. The effect of grain size on detrital modes: a test of the Gazzi-Dickinson point-counting method. J. Sediment. Res. 54 (1), 103–116. https://doi.org/10.1306/212F83B9-2B24-11D7-8648000102C1865D.
Israeli, Y., Emmanuel, S., 2018. Impact of grain size and rock composition on simulated rock weathering. Earth Surf. Dyn. 6 (2), 319–327. https://doi.org/10.5194/esurf-6-319-2018.
Ji, H., Tao, H., Wang, Q., Ma, D., Hao, L., 2019. Petrography, geochemistry, and geochronology of lower Jurassic sedimentary rocks from the Northern Tianshan (West Bogda area), Northwest China: implications for provenance and tectonic evolution. Geol. J. 54 (3), 1688–1714. https://doi.org/10.1002/gj.3263.
Jian, X., Guan, P., Zhang, W., Feng, F., 2013. Geochemistry of Mesozoic and Cenozoic sediments in the northern Qaidam basin, northeastern Tibetan Plateau: implications for provenance and weathering. Chem. Geol. 360, 74–88. https://doi.org/10.1016/j.chemgeo.2013.10.011.
Jian, X., Fu, L., Wang, P., Guan, P., Zhang, W., Fu, H., Mei, H., 2023. Sediment provenance of the Lulehe Formation in the Qaidam basin: Insight to initial Cenozoic deposition and deformation in northern Tibetan plateau. Basin Res. 35 (1), 271–294. https://doi.org/10.1111/bre.12712.

Jin, Z., Cao, J., Wu, J., Wang, S., 2006. A Rb/Sr record of catchment weathering response to Holocene climate change in Inner Mongolia. Earth Surf. Proc. Landforms: J. Br. Geomorphol. Res. Group. 31 (3), 285–291. https://doi.org/10.1002/esp.1243.
Kasper-Zubillaga, J.J., Martínez-Serrano, R.G., Arellano-Torres, E., Alvarez Sanchez, L.F., Patiño Andrade, D., Gonzalez Bermudez, A., Carlos-Delgado, L., 2021. Petrographic and geochemical analyses of dune sands from southeastern Mexico, Oaxaca, Mexico. Geol. J. 56 (6), 3012–3034. https://doi.org/10.1002/gj.4086.
Kassi, A.M., Grigsby, J.D., Khan, A.S., Kasi, A.K., 2015. Sandstone petrology and geochemistry of the Oligocene–Early Miocene Panjgur Formation, Makran accretionary wedge, southwest Pakistan: Implications for provenance, weathering and tectonic setting. J. Asian Earth Sci. 105, 192–207. https://doi.org/10.1016/j.jseaes.2015.03.021.
Keller, T., Håkansson, I., 2010. Estimation of reference bulk density from soil particle size distribution and soil organic matter content. Geoderma 154 (3–4), 398–406. https://doi.org/10.1016/j.geoderma.2009.11.013.
Krippner, A., Meinhold, G., Morton, A., Russell, E., von Eynatten, H., 2015. Grain-size dependence of garnet composition revealed by provenance signatures of modern stream sediments from the western Hohe Tauern (Austria). Sediment. Geol. 321, 25–38. https://doi.org/10.1016/j.sedgeo.2015.03.002.
Lafdani, E.K., Nia, A.M., Ahmadi, A., 2013. Daily suspended sediment load prediction using artificial neural networks and support vector machines. J. Hydrol. 478, 50–62. https://doi.org/10.1016/j.jhydrol.2012.11.048.
Land, M., Wust, R.A., Robert, C., Carter, R.M., 2010. Plio-Pleistocene paleoclimate in the Southwest Pacific as reflected in clay mineralogy and particle size at ODP Site 1119, SE New Zealand. Mar. Geol. 274 (1–4), 165–176. https://doi.org/10.1016/j.margeo.2010.04.001.
Le Pera, E., Arribas, J., Critelli, S., Tortosa, A., 2001. The effects of source rocks and chemical weathering on the petrogenesis of siliciclastic sand from the Neto River (Calabria, Italy): implications for provenance studies. Sedimentology 48 (2), 357–378. https://doi.org/10.1046/j.1365-3091.2001.00368.x.
Lee, S.Y., Kim, S.J., Baik, M.H., 2008. Chemical weathering of granite under acid rainfall environment, Korea. Environ. Geol. 55, 853–862. https://doi.org/10.1007/s00254-007-1037-7.
Li, C., Yang, S., 2010. Is chemical index of alteration (CIA) a reliable proxy for chemical weathering in global drainage basins? Am. J. Sci. 310 (2), 111–127. https://doi.org/10.2475/02.2010.03.
Li, C., Shi, X., Kao, S., Chen, M., Liu, Y., Fang, X., Lü, H., Zou, J., Liu, S., Qiao, S., 2012. Clay mineral composition and their sources for the fluvial sediments of Taiwanese rivers. Chin. Sci. Bull. 57, 673–681. https://doi.org/10.1007/s11434-011-4824-1.
Li, W., Qian, H., Xu, P., Hou, K., Zhang, Q., Chen, Y., Chen, J., Qu, W., Ren, W., 2023. Tracing sediment provenance in the Yellow River, China: insights from weathering, recycling, and rock compositions. Catena 220, 106727. https://doi.org/10.1016/j.catena.2022.106727.
Lim, D.I., Jung, H.S., Choi, J.Y., Yang, S., Ahn, K.S., 2006. Geochemical compositions of river and shelf sediments in the Yellow Sea: grain-size normalization and sediment provenance. Cont. Shelf Res. 26 (1), 15–24. https://doi.org/10.1016/j.csr.2005.10.001.
Liu, Z., Zhao, Y., Colin, C., Stattegger, K., Wiesner, M.G., Huh, C.-A., Zhang, Y., Li, X., Sompongchaiyakul, P., You, C.-F., Huang, C.-Y., Liu, J.T., Siringan, F.P., Le, K.P., Sathiamurthy, E., Hantoro, W.S., Liu, J., Tuo, S., Zhao, S., Zhou, S., He, Z., Wang, Y., Bunsomboonsakul, S., Li, Y., 2016. Source-to-sink transport processes of fluvial sediments in the South China Sea. Earth Sci. Rev. 153, 238–273. https://doi.org/10.1016/j.earscirev.2015.08.005.
Lu, S., Wu, B., Wang, H., Ouyang, N., Guo, S., 2012. Hydro-ecological impact of water conservancy projects in the Haihe River Basin. Acta Oecol. 44, 67–74. https://doi.org/10.1016/j.actao.2011.07.003.
Luo, X.X., Yang, S.L., Zhang, J., 2012. The impact of the three Gorges Dam on the downstream distribution and texture of sediments along the middle and lower Yangtze River (Changjiang) and its estuary, and subsequent sediment dispersal in the East China Sea. Geomorphology 179, 126–140. https://doi.org/10.1016/j.geomorph.2012.05.034.
Lv, D., Wang, L., Isbell, J.L., Lu, C., Li, P., Wang, Y., Zhang, Z., 2022. Records of chemical weathering and volcanism linked to paleoclimate transition during the late Paleozoic Icehouse. Glob. Planet. Chang. 217, 103934. https://doi.org/10.1016/j.gloplacha.2022.103934.
Lyu, H., Lu, H., 2024. Precipitation is the main control on the global distribution of soil clay minerals. Earth Sci. Rev., 104891 https://doi.org/10.1016/j.earscirev.2024.104891.
Ma, J.L., Wei, G.J., Xu, Y.G., Long, W.G., Sun, W.D., 2007. Mobilization and re-distribution of major and trace elements during extreme weathering of basalt in Hainan Island, South China. Geochim. Cosmochim. Acta 71 (13), 3223–3237. https://doi.org/10.1016/j.gca.2007.03.035.
Maggi, F., 2013. The settling velocity of mineral, biomineral, and biological particles and aggregates in water. J. Geophys. Res. Oceans 118 (4), 2118–2132. https://doi.org/10.1002/jgrc.20086.
Manassero, M., Camilión, C., Poiré, D., Da Silva, M., Ronco, A., 2008. Grain size analysis and clay mineral associations in bottom sediments from Paraná River Basin. Latin Am. J. Sedimentol. Basin Anal. 15 (2), 125–137.
Mei, H., Jian, X., Zhang, W., Fu, H., Zhang, S., 2021. Behavioral differences between weathering and pedogenesis in a subtropical humid granitic terrain: implications for chemical weathering intensity evaluation. Catena 203, 105368. https://doi.org/10.1016/j.catena.2021.105368.
Muhs, D.R., 2004. Mineralogical maturity in dunefields of North America, Africa and Australia. Geomorphology 59 (1–4), 247–269. https://doi.org/10.1016/j.geomorph.2003.07.020.
Mutema, M., Chaplot, V., Jewitt, G., Chivenge, P., Blöschl, G., 2015. Annual water, sediment, nutrient, and organic carbon fluxes in river basins: a global meta-analysis as a function of scale. Water Resour. Res. 51 (11), 8949–8972. https://doi.org/10.1002/2014WR016668.
Nemirovskaya, I.A., Shevchenko, V.P., 2020. Organic compounds and suspended particulate matter in snow of high latitude areas (Arctic and Antarctic). Atmosphere 11 (9), 928. https://doi.org/10.3390/atmos11S10090928.
Nesbitt, H., Young, G.M., 1982. Early Proterozoic climates and plate motions inferred from major element chemistry of lutites. Nature 299 (5885), 715–717. https://doi.org/10.1038/299715a0.
Nesbitt, H.W., Young, G.M., McLennan, S.M., Keays, R.R., 1996. Effects of chemical weathering and sorting on the petrogenesis of siliciclastic sediments, with implications for provenance studies. J. Geol. 104 (5), 525–542. https://doi.org/10.1086/629850.
Nyakairu, G.W.A., Koeberl, C., 2001. Mineralogical and chemical composition and distribution of rare earth elements in clay-rich sediments from Central Uganda. Geochem. J. 35 (1), 13–28. https://doi.org/10.2343/geochemj.35.13.
Pan, B., Pang, H., Zhang, D., Guan, Q., Wang, L., Li, F., Guan, W.Q., Cai, A., Sun, X., 2015. Sediment grain-size characteristics and its source implication in the Ningxia–Inner Mongolia sections on the upper reaches of the Yellow River. Geomorphology 246, 255–262. https://doi.org/10.1016/j.geomorph.2015.06.028.
Parker, A., 1970. An index of weathering for silicate rocks. Geol. Mag. 107 (6), 501–504. https://doi.org/10.1017/S0016756800058581.
Peel, M.C., Finlayson, B.L., McMahon, T.A., 2007. Updated world map of the Köppen-Geiger climate classification. Hydrol. Earth Syst. Sci. 11 (5), 1633–1644. https://doi.org/10.5194/hess-11-1633-2007.
Peng, G., Xiang, N., Lv, S.Q., Zhang, G.C., 2014. Fractal characterization of soil particle-size distribution under different land-use patterns in the Yellow River Delta Wetland in China. J. Soils Sediments 14, 1116–1122. https://doi.org/10.1007/s11368-014-0876-6.
Penman, D.E., Rugenstein, J.K.C., Ibarra, D.E., Winnick, M.J., 2020. Silicate weathering as a feedback and forcing in Earth's climate and carbon cycle. Earth Sci. Rev. 209, 103298. https://doi.org/10.1016/j.earscirev.2020.103298.
Peucker-Ehrenbrink, B., Miller, M.W., 2004. Quantitative bedrock geology of east and Southeast Asia (Brunei, Cambodia, eastern and southeastern China, East Timor, Indonesia, Japan, Laos, Malaysia, Myanmar, North Korea, Papua New Guinea, Philippines, far-eastern Russia, Singapore, South Korea, Taiwan, Thailand, Vietnam). Geochemistry, Geophysics, Geosystems 5 (1). https://doi.org/10.1029/2003GC000619.
Phillips, S.C., Littler, K., 2022. Comparison of sediment composition by smear slides to quantitative shipboard data: a case study on the utility of smear slide percent estimates, IODP Expedition 353, northern Indian Ocean. Sci. Drill. 30, 59–74. https://doi.org/10.5194/sd-30-59-2022.
Pollet-Villard, M., Daval, D., Fritz, B., Knauss, K.G., Schäfer, G., Ackerer, P., 2016. Influence of etch pit development on the surface area and dissolution kinetics of the orthoclase (001) surface. Chem. Geol. 447, 79–92. https://doi.org/10.1016/j.chemgeo.2016.09.038.
Qi, Y.H., Gong, Y.Z., Wu, F., Lu, Y., Cheng, W., Huang, F., Yu, H.M., 2022. Coupled variations in V-Fe abundances and isotope compositions in latosols: Implications for V mobilization during chemical weathering. Geochim. Cosmochim. Acta 320, 26–40. https://doi.org/10.1016/j.gca.2021.12.028.
Qin, Y.C., Mei, X., Jiang, X., Luan, X., Zhou, L., Zhu, X., 2021. Sediment provenance and tidal current-driven recycling of Yellow River detritus in the Bohai Sea, China. Mar. Geol. 436, 106473. https://doi.org/10.1016/j.margeo.2021.106473.
Roda-Boluda, D.C., D'Arcy, M., McDonald, J., Whittaker, A.C., 2018. Lithological controls on hillslope sediment supply: insights from landslide activity and grain size distributions. Earth Surface Processes and Landforms 43 (5), 956–977. https://doi.org/10.1002/esp.4281.
Rieu, R., Allen, P.A., Plotze, M., Pettke, T., 2007. Compositional and mineralogical variations in a Neoproterozoic glacially influenced succession, Mirbat area, South Oman: Implications for paleoweathering conditions. Precambrian Res. 154 (3–4), 248–265. https://doi.org/10.1016/j.precamres.2007.01.003.
Roser, B.P., Korsch, R.J., 1988. Provenance signatures of sandstone-mudstone suites determined using discriminant function analysis of major-element data. Chem. Geol. 67 (1–2), 119–139. https://doi.org/10.1016/0009-2541(88)90010-1.
Schulz, M.S., White, A.F., 1999. Chemical weathering in a tropical watershed, Luquillo Mountains, Puerto Rico III: quartz dissolution rates. Geochim. Cosmochim. Acta 63 (3–4), 337–350. https://doi.org/10.1016/S0016-7037(99)00056-3.
Setti, M., López-Galindo, A., Padoan, M., Garzanti, E., 2014. Clay mineralogy in southern Africa river muds. Clay Miner. 49 (5), 717–733. https://doi.org/10.1180/claymin.2014.049.5.08.
Shangguan, W., Dai, Y., Liu, B., Zhu, A., Duan, Q., Wu, L., Zhang, Y., 2013. A China data set of soil properties for land surface modeling. J. Adv. Model. Earth Syst. 5 (2), 212–224. https://doi.org/10.1002/jame.20026.
Shao, J., Yang, S., 2012. Does chemical index of alteration (CIA) reflect silicate weathering and monsoonal climate in the Changjiang River basin? Chin. Sci. Bull. 57, 1178–1187. https://doi.org/10.1007/s11434-011-4954-5.
Shao, L., Qiao, P., Zhao, M., Li, Q., Wu, M., Pang, X., Zhang, H., 2016. Depositional characteristics of the northern South China Sea in response to the evolution of the Pearl River. Geol. Soc. Lond. Spec. Publ. 429 (1), 31–44. https://doi.org/10.1144/SP429.2.
Shen, X., Jian, X., Zhang, W., Guan, P., 2024. Grain textural bias in detrital single-mineral provenance studies. Sediment. Geol. 471, 106731. https://doi.org/10.1016/j.sedgeo.2024.106731.
Singleton, A.A., Schmidt, A.H., Bierman, P.R., Rood, D.H., Neilson, T.B., Greene, E.S., Bower, J.A., Perdrial, N., 2017. Effects of grain size, mineralogy, and acid-

extractable grain coatings on the distribution of the fallout radionuclides 7Be, 10Be, 137Cs, and 210Pb in river sediment. Geochim. Cosmochim. Acta 197, 71–86. https://doi.org/10.1016/j.gca.2016.10.007.
Song, Q., Hong, H., Algeo, T.J., Fang, Q., Zhao, C., Liu, C., Xu, Y., 2023. Clay mineralogy mediated by pH and chemical weathering intensity of Permian–Triassic boundary K-bentonites at Dongpan (Guangxi, South China). Chem. Geol. 617, 121262. https://doi.org/10.1016/j.chemgeo.2022.121262.
Spalletti, L.A., Queralt, I., Matheos, S.D., Colombo, F., Maggi, J., 2008. Sedimentary petrology and geochemistry of siliciclastic rocks from the upper Jurassic Tordillo Formation (Neuquén Basin, western Argentina): implications for provenance and tectonic setting. J. S. Am. Earth Sci. 25 (4), 440–463. https://doi.org/10.1016/j.jsames.2007.08.005.
Stokes, G.G., 1850. On the effect of the internal Friction of Fluids onthe Motion of Pendulums, Transactions of the Cambridge Philosophi-cal Society IX, p. 8, reprinted in Mathematical and Physical Papers, 3, pp. 1–86.
Stutenbecker, L., Mark, C., Resentini, A., 2024. Editorial to the special collection "controls and biasing factors in sediment generation, routing, and provenance: models, methods, and case studies". J. Geophys. Res. Earth 129 (8), e2024JF007874. https://doi.org/10.1029/2024JF007874.
Su, N., Wu, Z., Yang, S., Xu, J., 2022. Re-assessing the effect of differential weathering of minerals on strontium stable isotope behavior during granodiorite weathering. Chem. Geol. 613, 121160. https://doi.org/10.1016/j.chemgeo.2022.121160.
Swärd, H., O'Regan, M., Pearce, C., Semiletov, I., Stranne, C., Tarras, H., Jakobsson, M., 2018. Sedimentary proxies for Pacific water inflow through the Herald Canyon, western Arctic Ocean. Arktos 4, 1–13. https://doi.org/10.1007/s41063-018-0055-x.
Szczuciński, W., Jagodziński, R., Hanebuth, T.J., Stattegger, K., Wetzel, A., Mitręga, M., Unverricht, D., Van Phach, P., 2013. Modern sedimentation and sediment dispersal pattern on the continental shelf off the Mekong River delta, South China Sea. Glob. Planet. Chang. 110, 195–213. https://doi.org/10.1016/j.gloplacha.2013.08.019.
Teng, F.Z., Hu, Y., Ma, J.L., Wei, G.J., Rudnick, R.L., 2020. Potassium isotope fractionation during continental weathering and implications for global K isotopic balance. Geochim. Cosmochim. Acta 278, 261–271. https://doi.org/10.1016/j.gca.2020.02.029.
Thorpe, M.T., Hurowitz, J.A., 2020. Unraveling sedimentary processes in fluvial sediments from two basalt dominated watersheds in northern Idaho, USA. Chem. Geol. 550, 119673. https://doi.org/10.1016/j.chemgeo.2020.119673.
Thorpe, M.T., Hurowitz, J.A., Dehouck, E., 2019. Sediment geochemistry and mineralogy from a glacial terrain river system in Southwest Iceland. Geochim. Cosmochim. Acta 263, 140–166. https://doi.org/10.1016/j.gca.2019.08.003.
Tian, S., Li, Z., Wang, Z., Jiang, E., Wang, W., Sun, M., 2021. Mineral composition and particle size distribution of river sediment and loess in the middle and lower Yellow River. Intern. J. Sed. Res. 36 (3), 392–400. https://doi.org/10.1016/j.ijsrc.2020.07.008.
Tolosana-Delgado, R., von Eynatten, H., 2009. Grain-size control on petrographic composition of sediments: compositional regression and rounded zeros. Math. Geosci. 41, 869–886. https://doi.org/10.1007/s11S10004-009-9216-6.
Van De Kamp, P.C., 2010. Arkose, subarkose, quartz sand, and associated muds derived from felsic plutonic rocks in glacial to tropical humid climates. Journal of Sedimentary Research 80 (10), 895–918. https://doi.org/10.2110/jsr.2010.081.
Venkatramanan, S., Ramkumar, T., Anithamary, I., 2013. Distribution of grain size, clay mineralogy and organic matter of surface sediments from Tirumalairajanar Estuary, Tamilnadu, east coast of India. Arab. J. Geosci. 6, 1371–1380. https://doi.org/10.1007/s12517-011-0423-3.
Wan, S., Li, A., Clift, P.D., Stuut, J.B.W., 2007. Development of the East Asian monsoon: mineralogical and sedimentologic records in the northern South China Sea since 20 Ma. Palaeogeogr. Palaeoclimatol. Palaeoecol. 254 (3–4), 561–582. https://doi.org/10.1016/j.palaeo.2007.07.009.
Wang, L., 2024. Feasibility Evaluation of Clay Minerals as Indicators of Chemical Weathering and climate Change [D] (in Chinese). Xiamen University. 1–94.
Wang, L., Jian, X., Fu, H., Zhang, W., Shang, F., Fu, L., 2023. Decoupled local climate and chemical weathering intensity of fine-grained siliciclastic sediments from a paleo-megalake: an example from the Qaidam basin, northern Tibetan Plateau. Sediment. Geol. 454, 106462. https://doi.org/10.1016/j.sedgeo.2023.106462.
Wang, S., Zhang, N., Chen, H., Li, L., Yan, W., 2014. The surface sediment types and their rare earth element characteristics from the continental shelf of the northern South China Sea. Cont. Shelf Res. 88, 185–202. https://doi.org/10.1016/j.csr.2014.08.005.
Wang, W., Zhou, M.F., 2013. Petrological and geochemical constraints on provenance, paleoweathering, and tectonic setting of the Neoproterozoic sedimentary basin in the eastern Jiangnan Orogen, South China. J. Sediment. Res. 83 (11), 975–994. https://doi.org/10.2110/jsr.2013.74.
Wang, Z., Ma, J., Li, J., Wei, G., Zeng, T., Li, L., Zhang, L., Deng, W., Xie, L., Liu, Z., 2018. Fe (hydro) oxide controls Mo isotope fractionation during the weathering of granite. Geochim. Cosmochim. Acta 226, 1–17. https://doi.org/10.1016/j.gca.2018.01.032.
Wang, Z.B., Li, R.H., Yang, S.Y., Bai, F.L., Mei, X., Zhang, J., Lu, K., 2019. Comparison of detrital mineral compositions between stream sediments of the Yangtze River (Changjiang) and the Yellow River (Huanghe) and their provenance implication. China Geol. 2 (2), 169–178. https://doi.org/10.31035/cg2018065.
Wani, H., Mondal, M.E.A., 2010. Petrological and geochemical evidence of the Paleoproterozoic and the Meso-Neoproterozoic sedimentary rocks of the Bastar craton, Indian Peninsula: Implications on paleoweathering and Proterozoic crustal evolution. J. Asian Earth Sci. 38 (5), 220–232. https://doi.org/10.1016/j.jseaes.2010.01.003.
Warr, L.N., 2022. Earth's clay mineral inventory and its climate interaction: a quantitative assessment. Earth Sci. Rev. 234, 104198. https://doi.org/10.1016/j.earscirev.2022.104198.
Warr, L.N., Grathoff, G.H., Haberzettl, T., 2024. The Clay Mineral Alteration Index (CMAI) as an improved indicator of climate change. Appl. Clay Sci. 256 (2024), 107419. https://doi.org/10.1016/j.clay.2024.107419.
White, A.F., Bullen, T.D., Schulz, M.S., Blum, A.E., Huntington, T.G., Peters, N.E., 2001. Differential rates of feldspar weathering in granitic regoliths. Geochim. Cosmochim. Acta 65 (6), 847–869. https://doi.org/10.1016/S0016-7037(00)00577-9.
Wilson, M.J., 2004. Weathering of the primary rock-forming minerals: processes, products and rates. Clay Miner. 39 (3), 233–266. https://doi.org/10.1180/0009855043930133.
Worthington, S.R., Davies, G.J., Alexander Jr., E.C., 2016. Enhancement of bedrock permeability by weathering. Earth Sci. Rev. 160, 188–202. https://doi.org/10.1016/j.earscirev.2016.07.002.
Wu, B., Lang, X., Jiang, D., 2021. Köppen climate zones in China over the last 21,000 years. J. Geophys. Res. Atmos. 126 (6), e2020JD034310. https://doi.org/10.1029/2020JD034310.
Wu, K., Liu, S., Kandasamy, S., Jin, A., Lou, Z., Li, J., Wu, B., Wang, X.X., Mohamed, C.A., Shi, X., 2019. Grain-size effect on rare earth elements in Pahang River and Kelantan River, Peninsular Malaysia: Implications for sediment provenance in the southern South China Sea. Cont. Shelf Res. 189, 103977. https://doi.org/10.1016/j.csr.2019.103977.
Xiao, J., Jin, Z., Zhang, F., Wang, J., 2012. Major ion geochemistry of shallow groundwater in the Qinghai Lake catchment, NE Qinghai-Tibet Plateau. Environ. Earth Sci. 67, 1331–1344. https://doi.org/10.1007/s12665-012-1576-4.
Xiao, J., Song, Y., Li, Y., 2023. Comparison of quantitative X-ray diffraction mineral analysis methods. Minerals 13 (4), 566. https://doi.org/10.3390/min13040566.
Xie, Y., Yuan, F., Zhan, T., Kang, C., Chi, Y., 2018. Geochemical and isotopic characteristics of sediments for the Hulun Buir Sandy Land, Northeast China: implication for weathering, recycling and dust provenance. Catena 160, 170–184. https://doi.org/10.1016/j.catena.2017.09.008.
Xu, F., Hu, B., Dou, Y., Liu, X., Wan, S., Xu, Z., Tian, X., Liu, Z., Yin, X., Li, A., 2017. Sediment provenance and paleoenvironmental changes in the northwestern shelf mud area of the South China Sea since the mid-Holocene. Cont. Shelf Res. 144, 21–30. https://doi.org/10.1016/j.csr.2017.06.013.
Xu, G., Li, Z., Li, P., 2013. Fractal features of soil particle-size distribution and total soil nitrogen distribution in a typical watershed in the source area of the middle Dan River, China. Catena 101, 17–23. https://doi.org/10.1016/j.catena.2012.09.013.
Xu, X., Dong, C., Li, W., Zhou, X., 1999. Late Mesozoic intrusive complexes in the coastal area of Fujian, SE China: the significance of the gabbro-diorite–granite association. Lithos 46 (2), 299–315. https://doi.org/10.1016/S0024-4937(98)00087-5.
Yang, L., Zhang, F., Hu, Y., Zhan, Y., Deng, L., Huang, H., Sun, H., Wei, Y., Li, X., 2022. Seasonal variations of chemical weathering and CO2 consumption processes in the Headwater (Datong River Basin) of the Yellow River Draining the Tibetan Plateau. Front. Earth Sci. 10. https://doi.org/10.3389/feart.2022.909749.
Yang, Z.S., Zhao, X.H., Qiao, S.Q., Li, Y.H., Fan, D.J., 2008. Feldspar/Quartz(F/Q) Ratios as a Chemical Weathering Intensity Indicator in different Grain Size-Fractions of Sediments from the Changjiang and Huanghe Rivers to the Seas (in Chinese). Period. Ocean Univer. China. 38 (2), 244–250. https://doi.org/10.16441/j.cnki.hdxb.2008.02.014.
Yu, F., Switzer, A.D., Zheng, Z., Chen, B., Pile, J., Jol, H., Huang, Z.Q., Lau, A., 2024. Holocene geomorphological evolution of a sediment-starved coastal embayment in response to sea level change: Insights from the Qing'ao Embayment, southern China. Palaeogeogr. Palaeoclimatol. Palaeoecol. 633, 111895. https://doi.org/10.1016/j.palaeo.2023.111895.
Yuan, G., Cao, Y., Schulz, H.M., Hao, F., Gluyas, J., Liu, K., Yang, T., Wang, Y., Xi, K., Li, F., 2019. A review of feldspar alteration and its geological significance in sedimentary basins: from shallow aquifers to deep hydrocarbon reservoirs. Earth Sci. Rev. 191, 114–140. https://doi.org/10.1016/j.earscirev.2019.02.004.
Yusoff, Z.M., Ngwenya, B.T., Parsons, I., 2013. Mobility and fractionation of REEs during deep weathering of geochemically contrasting granites in a tropical setting, Malaysia. Chem. Geol. 349, 71–86. https://doi.org/10.1016/j.chemgeo.2013.04.016.
Zeroual, A., Assani, A.A., Meddi, M., Alkama, R., 2019. Assessment of climate change in Algeria from 1951 to 2098 using the Köppen-Geiger climate classification scheme. Clim. Dyn. 52, 227–243. https://doi.org/10.1007/s00382-018-4128-0.
Zhang, Y., Yu, S., He, S., Sun, P., Wu, F., Liu, Z., Zhu, H., Li, X., Zeng, P., 2021. New estimate of chemical weathering rate in Xijiang River Basin based on multi-model. Sci. Rep. 11 (1), 1–26. https://doi.org/10.1038/s41598-021-84602-1.
Zhao, D., Wan, S., Yu, Z., Huang, J., 2015. Distribution, enrichment and sources of heavy metals in surface sediments of Hainan Island rivers, China. Environ. Earth Sci. 74, 5097–5110. https://doi.org/10.1007/s12S11665-015-4522-4.
Zhong, Y., Chen, Z., Li, L., Liu, J., Li, G., Zheng, X., Wang, S., Mo, A., 2017. Bottom water hydrodynamic provinces and transport patterns of the northern South China Sea: evidence from grain size of the terrigenous sediments. Cont. Shelf Res. 140, 11–26. https://doi.org/10.1016/j.csr.2017.01.023.
Zhou, X., Li, A., Jiang, F., Lu, J., 2015. Effects of grain size distribution on mineralogical and chemical compositions: a case study from size-fractional sediments of the Huanghe (Yellow River) and Changjiang (Yangtze River). Geol. J. 50 (4), 414–433. https://doi.org/10.1002/gj.2546.
Zhou, X., Liu, D., Bu, H., Deng, L., Liu, H., Yuan, P., Du, P., Song, H., 2018. XRD-based quantitative analysis of clay minerals using reference intensity ratios, mineral

intensity factors, Rietveld, and full pattern summation methods: a critical review. Solid Earth Sci. 3 (1), 16–29. https://doi.org/10.1016/j.sesci.2017.12.002.
Zhu, C., 2005. In situ feldspar dissolution rates in an aquifer. Geochim. Cosmochim. Acta 69 (6), 1435–1453. https://doi.org/10.1016/j.gca.2004.09.005.
Zuffa, G.G., 1985. Optical analyses of arenites: Influence of methodology on compositional results. In: Provenance of Arenites. Springer Netherlands, Dordrecht, pp. 165–189. https://doi.org/10.1007/978-94-017-2809-6_8.